INVESTIGATING THE CORROSION BEHAVIOUR OF ZX10 MAGNESIUM ALLOY IN VARIOUS CORROSIVE MEDIA AND THE CORROSION RESISTANCE OF MAGNESIUM OXIDE COATINGS

A Thesis Submitted to the
College of Graduate and Postdoctoral Studies
In Partial Fulfillment of the Requirements
For the Degree of Master of Science
In the Department of Mechanical Engineering
University of Saskatchewan
Saskatoon

By
Zhen Xu

PERMISSION TO USE

In presenting this thesis in partial fulfillment of the requirements for a Postgraduate degree from the University of Saskatchewan, I agree that the Libraries of this University may make it freely available for inspection. I further agree that permission for copying of this thesis in any manner, in whole or in part, for scholarly purposes may be granted by Prof. Jerzy.A.Szpunar, the professor who supervised my thesis work or, in their absence, by the Head of the Department or the Dean of the College in which my thesis work was done. It is understood that any copying or publication or use of this thesis or parts thereof for financial gain shall not be allowed without my written permission. It is also understood that due recognition shall be given to me and to the University of Saskatchewan in any scholarly use which may be made of any material in my thesis.

Requests for permission to copy or to make other uses of materials in this thesis in whole or part should be addressed to:

Head of the Department of Mechanical Engineering

University of Saskatchewan

57 Campus Drive

Saskatoon, Saskatchewan S7N 5A9 Canada.

OR

Dean

College of Graduate and Postdoctoral Studies

University of Saskatchewan

116 Thorvaldson Building, 110 Science Place

Saskatoon, Saskatchewan S7N 5C9 Canada

ABSTRACT

At present, magnesium alloys are receiving considerable attention in the fields of computer parts, automotive, aerospace components, and biomedical applications because of their low density, high specific strength and bio-compatibility. Among them, the ZX10 magnesium alloy exhibits excellent mechanical properties. However, due to their poor corrosion resistance and insufficient mechanical properties when exposed to different aggressive environment, the engineering application of magnesium alloys is limited and requires appropriate surface treatment. This study, therefore, focused on the degradation behaviour of ZX10 magnesium alloy in different corrosive media at room temperature and the development of protective MgO coating on ZX10 magnesium alloy.

The degradation behaviour and corrosion rate of ZX10 magnesium alloy in different aggressive media with varying pH values, were investigated by employing the Tafel curve and electrochemical impedance techniques, and analyzed with the Scanning Electron Microscope (SEM). The chemistry and diffraction phases of adhering corrosion products were also investigated by utilizing the X-ray diffraction (XRD) technique. MgO coatings were electrodeposited on magnesium alloy using cathodic electrolytic method and subsequent calcination at different temperatures to improve the corrosion resistance. The protective performance of the MgO coatings was investigated by potentiodynamic polarization, and electrochemical impedance spectroscopy and a correlation was drawn between calcination temperature of coatings, corrosion resistance, and mechanical hardness. A modeled calcination mechanism, as it relates to barrier performance at low and high thermal conditions, has been illustrated based on collected experimental evidence.

Results showed that magnesium alloy demonstrated varying rates of corrosion and passivation within a range of pH of corrosion media. The acidic systems showed the highest rate of metal corrosion while the lowest corrosion rate was observed for the alkaline systems. Localized corrosion has been observed by SEM, while electrochemical impedance spectroscopy and potentiodynamic polarization techniques reveal increased anodic polarization and charge transfer, respectively. The metal uniformly corroded for each examined corrodent over an extended period of time; however, the early corrosion stages reveal localized formation of oxide films at grain boundaries.

The protective MgO coating was successfully developed and optimized on ZX10 magnesium alloy. The internal tensile stress was produced in electrodeposition because of the occlusion of hydrogen atoms in the coatings. Results showed that at calcination temperature of 250^{o}C, the internal tensile stress was released leading to crystallization of oxide coating layers with compact and continuous multi-layered micro-structures. At higher temperatures (around 500^{o}C), recrystallization of the MgO coating increased coating porosity and broadened inter-diffusion at micro-defects. Surface and bulk pores and cracks have been observed at 500^{o}C as clear evidence of the consequence of over-calcination. Enhanced corrosion resistance was observed for the MgO coatings obtained at 250^{o}C calcination temperature after chloride-induced corrosion tests and its corrosion current density is one thousand times smaller than that of bare magnesium alloy.

ACKNOWLEDGMENT

Many people have offered me valuable help in my thesis writing, including my supervisor, my advisory committee members, my group members and my parents.

Firstly, I would like to give my sincere gratitude to my supervisor, Prof. Jerzy Szpunar for the opportunity to finish my M.Sc. study under his guidance. His extraordinary patience, consistent encouragement, professional and scientific contributions to the success of my study benefited me a great deal. I thank Prof. Szpunar for granting me the permission to use his SEM and EBSD facility. Without his strong support, this thesis could not have reached its present form. Also, I appreciate the contributions of my advisory committee members, Prof. Akindele Odeshi, Prof. Duncan Cree and Prof. Ding-Yu Peng. Their time, advice, valuable comments greatly contributed to the success of this study.

Then, I would like to express my heartfelt gratitude to Dr. Ubong for his time, patient guidance, insightful and valuable advice which have remarkably contributed to the success of this study. It is him that leaded me to this research area and helped me work out my problems during the difficult course of the thesis. I also like to express my gratitude to my group mates for their time and expert training on lab details and using the experiment techniques including Scanning Electron Microscopy (SEM), Electron Backscatter Diffraction (EBSD) and X-ray diffraction (XRD).

Finally, my thanks would go to my beloved family for their loving considerations and great confidence in me these years. They have always been encouraging me and giving me helpful advice through my graduate studies. It is of great help for me to finish my M.Sc. study.

TABLE OF CONTENTS

LIST OF TABLES

LIST OF FIGURES

LIST OF ABBREVIATIONS AND SYMBOLS

ABBREVIATIONS

Mg	Magnesium
MgO	Magnesium Oxide
XPS	X-ray photoelectron spectroscopy
EIS	Electrochemical impedance spectroscopy
SEM	Scanning electron microscope/microscopy
TEM	Transmission electron microscope/microscopy
EDS	Energy dispersive X-ray spectroscopy
EBSD	Electron backscattered diffraction
XRD	X-ray diffraction
HV	Vickers hardness

SYMBOLS

v	Corrosion rate, mpy (mils per year)
Δw	Weight loss, g
A	Average surface area, cm^2
t	Immersion time, h
ρ	Density of Mg, g/cm^3

CHAPTER ONE

INTRODUCTION

1.1 Overview

Magnesium (Mg) is the third most abundant element dissolved in seawater and it is also the eighth most abundant element in the Earth's crust [1]. It has good specific strength and low density, only two-thirds that of Al, so Mg and its alloys can be applied in many fields, including computer parts, mobile phones, aerospace components and handheld tools. Magnesium alloys are also receiving significant attention in the automotive industry because of their high strength to weight ratio in addition to other advantages [2]. Because of the biodegradability and bio-compatibility of magnesium alloys in human physiological environments, they are also quite attractive in applications in biomedical implants (such as hard tissue replacement, bone implants and stent applications) [3]. Their degradable property allows to avoid a second surgery after the healing of tissue, and they have a closer Young's modulus to human bones compared to other common implant materials such as stainless steels and titanium alloys [4]. From the point of view of mechanical strength, most biodegradable Mg implants deployed in modern biomedical applications are considered more similar to bones than permanent stainless-steel implants and Ti_6Al_4V alloys [5,6-9]. Magnesium alloys are mechanically advantageous as implants because of their unique stiffness, specific strengths and good machinability.

However, Mg-based alloys have poor corrosion resistance and their susceptibility to corrosion significantly limit many other applications. Their poor corrosion resistance is mainly due to the microstructure and the localized galvanic corrosion caused by the impurities in the magnesium alloy [10]. They are chemically active, especially under internal galvanic corrosion. Both the

severe pitting corrosion on the metal surface and galvanic corrosion decrease mechanical stability and results in an unattractive appearance of the metal [11]. Because of the pitting corrosion at grain boundaries in the human physiological environment, the mechanical integrity of magnesium alloys is frequently destroyed in a short time after implantation before healing the tissue. The grain boundaries, as well as the inhomogeneous distribution of second phases, largely accounts for the pitting corrosion [12]. Therefore, appropriate surface treatment is essential for the protection of magnesium alloys in engineering applications.

The corrosion behaviour of magnesium alloys is significantly dependent on the microstructure, particularly on the amount and distribution of the intermetallic phases and the grain size [1]. So far, several studies [12] have investigated the coating degradation and degradation of magnesium alloy in biological fluids. However, there is very little literature on the degradation behaviour of magnesium alloy in other corrosive media, especially alkali and acid. This study employs the Tafel curves and electrochemical impedance techniques together with Scanning Electron Microscope (SEM) to study the degradation behaviour and corrosion rate of magnesium alloy. The phases of adhering corrosion products were investigated using XRD technique. The corrosion mechanism of magnesium alloy in sodium chloride was explored in details.

The high affinity of magnesium alloys to corrosion in chloride rich body fluids as well as the hydrogen accumulation contributes to costly maintenance of Mg implants while the increase in local pH (alkalinity) between tissues also leads to the implant loosening [5,13]. Depending on the environments they are utilized, magnesium alloys readily passivate by forming thin layers of oxides and hydroxides on their surfaces. However, when the rate of corrosion exceeds passivation, significant material is lost. Metal surface treatment with protective coatings has been identified as an effective mitigation against corrosion. Recent developments in electroplating, anodizing, laser-

assisted surface alloying and hybrid coatings for magnesium alloys have led to continued progress in the coating designs [14].

The coating of MgO on magnesium alloy is an effective mitigation tool to control the corrosion rate in bio-medical applications. First, MgO coating is bio-compatible, which means the coating can carry out its intended function without inducing harmful or toxic species in the human body, so it is safe for medical use. Besides, MgO film has excellent compatibility with the magnesium alloy substrate and also good adhesion to magnesium alloy because it is naturally formed on the surface of magnesium alloy and can provide good corrosion resistance. The MgO coating, which is produced by electrodeposition has several advantages compared with other coatings used for magnesium. These advantages include low cost, purity of the coating phase, simple equipment for the coating deposition, high deposition rate, and the ability to coat the substrate with complex shapes. For this reason in the present study, MgO was developed on magnesium alloy by electrodeposition and subsequent calcination at a defined temperature range. Moreover, the effect of different calcination temperature on the corrosion barrier performance of each coating is investigated. Comprehensive corrosion performance tests are conducted in aerated NaCl solution at room temperature for Mg-Zn-Ca type alloy as the test substrate. As far as we know for Mg-Zn-Ca alloys, there has been no experimental attempt to investigate corrosion in chloride media. Lei *et al.* [14] investigated the corrosion resistance of MgO coating on ZX10 magnesium alloy by anodization in the KOH solution. The authors identified evidence of MgO conversion from $Mg(OH)_2$ during calcination at 450°C. The rate of nucleation and growth of coatings was enhanced in 10 M (mol/L) KOH, and these coatings had improved corrosion resistance of the magnesium alloy substrate relative to the bare metal. Cai *et al*. [15] used current impedimetric method to investigate the anodic oxidation of Mg in KOH. Anodization of the substrate caused not only active

dissolution but also passivation. The dissolution of Mg was controlled by the charge transfer process at the active region, while the deposition of $Mg(OH)_2$ was the dominant reaction at the passive region. As explained by the authors, a secondary oxidation reaction where Mg spontaneously oxidized to MgO can precede these primary oxidation steps. Through recording impedance curves at varying amplitudes, the authors explained the electrochemistry of Mg corrosion through anodic polarization in 6 M KOH solution at different scan rates. In addition to electrodeposition, micro-arc oxidation as a plasma anodizing technique has also made significant progress in the development of coating technology [16,17]. The electrolytic deposition of MgO coatings on nickel superalloy has also been investigated by Szpunar *et al*. [18]. However, the effect of heat treatment on the coating barrier performance is still not well known and needs to be studied. There is some other literature reporting the influence of calcination temperature on the corrosion resistance of Ni-B-W [19], Ni-W-Cr-P [20], Al-Si [21] and Ni-B-Mo [22] coatings produced using various methods.

1.2 Motivation

At present, due to their poor corrosion resistance, the engineering application of magnesium alloys is quite limited especially when exposed to aggressive environments such as those including chloride [Cl^-] ions [32]. Generally, magnesium alloys degrade at a very high rate in the marine environments of pH (7.4–7.6) due to its high electrochemical activity losing their mechanical integrity. Hence, the future improvement in practical applications is preceded by understanding the dynamic degradation behaviour of magnesium alloys in aggressive environments. The promising future of Mg and its alloys is dependent mainly on improving the corrosion resistance in corrosive environments [1]. There is much literature on corrosion of magnesium alloy for

biodegradable implants today as magnesium alloys are excellent implant materials due to their high yield strength and the similar elastic modulus to that of human bones, which helps reduce stress-shielding effect [44]. However, most of the research was carried out on AZ31 or 91 magnesium alloy [30,33-34,42-43] under the corrosive environment which contains corrosive ions like HPO_4^{2-}, Cl^-, HCO_3^{2-} and SO_4^{2-} as well as cations like Mg^{2+}, Na^+ and Ca^{2+} to simulate in body fluid solution [45]. More recently, research on ZX alloys has resulted in the development of $MgZn_1Ca_{0.3}$(ZX10) magnesium alloy, that exhibits slow and homogeneous degradation with no significant hydrogen bubble formation and excellent mechanical properties. As far as we know, no one has previously reported the degradation behaviour of ZX10 magnesium alloy in different corrosive media in a systematic way. There is only a limited literature on the corrosion mechanism of magnesium alloy in acidic or alkali environment. Hence, the degradation behaviour of ZX10 magnesium alloys and its corrosion mechanism are reported here.

In-depth corrosion performance tests are carried out in 3.5 wt% NaCl solution at room temperature using ZX10 Mg-Zn-Ca alloy as the substrate. To the best of our knowledge, there is no such experimental study for ZX10 Mg-Zn-Ca alloys in chloride media. In the present study, the electrodeposition of MgO coatings was optimized and the protective performance of MgO coating on ZX10 magnesium alloy was also investigated.

1.3 Research objectives

The overall goal of this research is to establish the degradation behaviour of ZX10 magnesium alloy in different corrosive media and to develop protective MgO coating on magnesium alloy. The structure of the coatings will be optimized to improve the corrosion resistance of the investigated alloy. The specific objectives are listed below:

1. To describe the corrosion behaviour of ZX10 magnesium alloy in different aggressive media with varying pH values (acid, basic and neutral).
2. To develop and optimize MgO coating on ZX10 magnesium alloy by electrodeposition and subsequent calcination to improve the corrosion resistance.
3. To investigate the protective performance of the calcinated MgO coating on magnesium alloy.
4. To compare the mechanical hardness of MgO coatings calcinated at different temperatures.
5. To illustrate the coating calcination mechanism related to barrier performance.

1.4 Thesis arrangement

The current chapter, Chapter One, contains an overview, the motivations and objectives of this research. A summary of some of the previous work by other researchers in areas related to this study is provided as a literature review in Chapter Two. Detailed information about the investigated magnesium alloys and experimental procedures are introduced in Chapter Three. Chapter Four contains the results and discussion, while Chapter Five contains the summary and the conclusions drawn from this study.

CHAPTER TWO

LITERATURE REVIEW

2.1 Magnesium and its alloy

2.1.1 Zinc-containing and Calcium-containing magnesium alloy

Magnesium (Mg) and its alloys have quite a few excellent properties such as high specific strength and low density, which can be beneficial for application in aerospace and automotive industries where the fuel consumption and emission of greenhouse gas is very high [63]. Besides, other properties like its excellent fluidity in casting, good damping capability, low heat capacity, good electric shielding effect, satisfactory heat conductivity and non-toxicity makes Mg and its alloys quite attractive for many industrial applications [62]. However, the applications in the areas of automotive, electronics and aerospace industries are facing the crucial challenge due to its poor corrosion resistance. One of the most useful techniques for improving the corrosion resistance of Mg is alloying. From the viewpoint of the materials, the alloying metal usually has better corrosion behaviour compared to pure metal [47]. A smaller amount of Zinc in magnesium alloy can improve the strength because of solid solution strengthening, and at the same time, it can also contribute to the castability. However, a larger amount of Zn (>2 wt%) can cause embrittlement when combining with aluminum [47]. Also, Zn can increase age-hardening response by producing intermetallic compounds as well as refining the grain size. Compared with the impurities like Fe and Ni in magnesium alloys, zinc is more anodic, so it contributes to overcoming the harmful corrosion effects. Zn is also found in the human body, so it is safe for biomedical use. Therefore, Zn-containing magnesium alloys are well known as the most suitable candidate for biomedical applications [2].

Calcium (Ca) element in magnesium alloy contributes to the reduction of Mg oxidation and Ca addition also produces Ca-based intermetallic compounds by eutectic reactions. Kim *et al*. [48] studied the effect of Ca addition on the oxidation of Al-Mg alloy, and he found that there were two kinds of Ca-based intermetallic compounds formed: Laves_C36 and Al_4Ca phases. This results in the formation of multi-element oxides, which contain Mg, Al, and Ca. These oxides could eventually slow down the procedure of outward diffusion of Mg atoms and help to form a compact oxide protective layer [48]. As Ca is the main component in human bones, the addition of Ca element is beneficial for bone curing. Besides, the Ca element in magnesium alloy helps to strengthen the alloy by solid solution strengthening and precipitation strengthening.

To some extent, Ca can refine the grains leading to grain boundary strengthening. For example, in binary Mg-Ca alloys, the formed Laves phase Mg_2Ca improves creep-resistance because of solid solution strengthening, precipitation strengthening as well as grain boundary pinning. However, there are some problems if the amounts of Ca are over 1 wt% in the process of alloy casting, such as sticking or hot tearing [47].

ZX10 magnesium alloy exhibits slow and homogeneous degradation with no significant hydrogen bubble formation and excellent mechanical properties. The main philosophy behind the development of the ZX10 magnesium alloy was to keep the Zn and Ca contents to low enough levels in order to produce a very fine dispersion of intermetallic particles that improve the strength while minimising the localized dissolution/pitting due to the anodic nature of the intermetallics formed (Mg_2Ca).

2.1.2 The challenge of magnesium alloy

The application of magnesium alloys in practice is critically challenged by their rapid corrosion

rates and its effect on mechanical properties, especially when exposed to aggressive environments such as those of chloride [Cl^-] ions [32]. Magnesium alloys tend to corrode very quickly in the marine environments of pH (7.4–7.6) due to its high electrochemical activity, thereby losing their mechanical integrity. Therefore, understanding the dynamic degradation behaviour of magnesium alloys in vitro and in vivo is the first step to the future practical applications. The promising future of Mg and its alloys depends on being able to control the corrosion rate [1]. Lopez *et al*. [1] discussed the corrosion behaviour of AZ31 magnesium alloy with different grain sizes in simulated biological fluids, including NaCl solution and phosphate-buffer solution but not in alkali or acidic solutions. The microstructure and degradation of carbon containing micro-arc oxidation (MAO-C) coating on magnesium alloy wires treated with micro-arc oxidation were reported by Hua *et al*. [32]. The effect of heat treatment on the microstructure and corrosion behaviour of Mg-Zn alloys was investigated by Rad *et al*. [2]. After exposing Mg-based alloy to the simulated body fluid (SBF) solution, at first magnesium alloys are dissolved, and simultaneously a corrosion product begins to deposit on the sample surface. Magnesium alloy now is widely used in biodegradable implants mainly because it has high yield strength and low elastic modulus (41-45 GPa) which is close to that of human bones (3-20 GPa), and that helps to avoid stress- shielding effect [44]. There are many publications on corrosion of magnesium alloy for biodegradable implants application. However, most of them are on AZ31, or AZ91 magnesium alloy [30,33-34,42-43] and the environment is close to human body fluid solution, which contains ions like HPO_4^{2-}, Cl^-, HCO_3^{2-} and SO_4^{2-} as well as cations like Mg^{2+}, Na^+ and Ca^{2+} [45]. There is only a limited number of studies on the corrosion mechanism of magnesium alloy in acidic or alkali environment, and no one has previously systematically reported the corrosion of ZX10 magnesium alloy in different corrosive media. Our research gives a comprehensive study of the degradation behaviour of magnesium

alloy and its corrosion mechanism in different corrosive media, including salt, acid and alkali.

2.2 The corrosion of magnesium and its alloys

2.2.1 The corrosion types of magnesium and its alloys

Magnesium and its alloys suffer from several kinds of corrosion, including galvanic corrosion, intergranular corrosion, localized corrosion, stress corrosion cracking (SCC), corrosion fatigue as well as the corrosion at elevated temperatures [55]. In applications, localized corrosion and non-uniform damage are the biggest corrosion problem. The corrosion damage in Mg and its alloys cannot be uniform due to the inevitable electrochemical or micro-galvanic non-uniformity. Due to the presence of impurity particles and the second phase particles as well as the differences of grain orientation and alloying element distribution in the matrix phase, the distribution of both the micro-anodes and micro-cathodes is uneven in the magnesium alloys. The unevenness can eventually cause localized and non-uniform corrosion damage. Also, more intense anodic and cathodic reactions in a corroded area than in not corroded area lead to the non-uniform corrosion progresses in some local areas. Sometimes a certain amount of localized corrosion even brings about the underlying corrosion, which is often seen in corroding magnesium alloys. Underlying corrosion of magnesium alloys may take place in a severe corrosion process. **Figure 2.1** explains the procedure of an underlying corrosion process induced by localized corrosion.

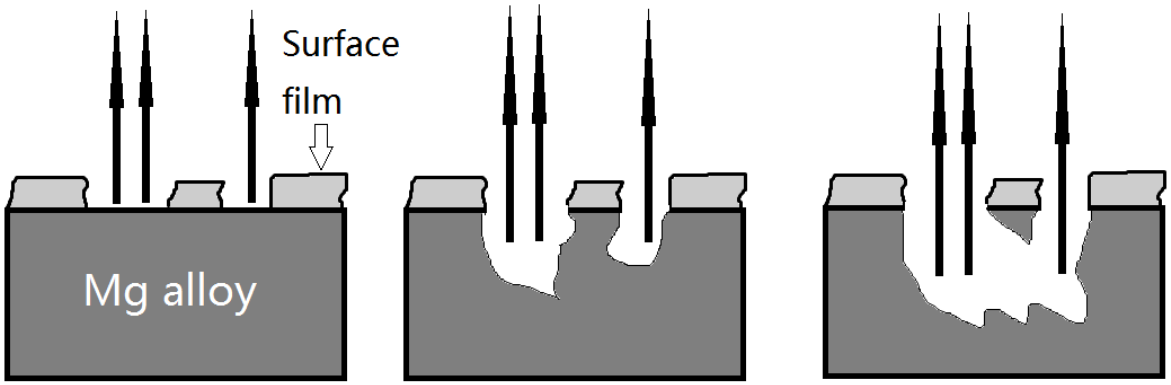

Figure 2.1. The procedure of localized corrosion and underlying corrosion

Even though localized corrosion is a significant corrosion form of magnesium alloy, it is not a process of pitting. In most environments, the localized corrosion of Mg is initiated from the oxide film-free areas, and it appears in the form of small irregular localized pits, which later spread over the magnesium alloy surface. Compared with typical pitting corrosion, the localized corrosion of magnesium alloys does not go deeply into the substrate. The reason is that the corrosion of magnesium alloys causes alkalization of the solution, and then the anodic dissolution of magnesium alloys at the tips of the corroding pits is reduced as a result of alkalization. Hence, an auto-catalytic corrosion cell cannot set up at the tips of corrosion to maintain a pitting procedure. Even though the corrosion spreading degree can be quite different for different alloys, this natural corrosion process, which is limited by itself, is likely to bring about quite widespread corrosion damage. The localized corrosion in magnesium alloy is not a real form of pitting process [50].

2.2.2 The reactions of magnesium in an aqueous solution

The following are a few reactions that may impact the corrosion of Mg in an aqueous solution [50]:

$Mg \rightarrow Mg^{2+} + 2e^-$ $\qquad E_0 = -2.363$ V

$Mg + 2OH^- \rightarrow Mg(OH)_2 + 2e^-$	$E_0 = –2.689$ V
$Mg \rightarrow Mg^+ + e^-$	$E_0 = –2.659$ V
$Mg + OH^- \rightarrow MgOH + e^-$	$E_0 = –3.140$ V
$Mg^+ \rightarrow Mg^{2+} + e^-$	$E_0 = –2.067$ V
$Mg^+ + 2OH^- \rightarrow Mg(OH)_2 + e^-$	$E_0 = –2.702$ V
$Mg^+ + 2H_2O \rightarrow Mg(OH)_2 + 2H^+ + e^-$	$E_0 = –1.065$ V
$MgOH + OH^- \rightarrow Mg(OH)^2 + e^-$	$E_0 = –2.240$ V
$MgH_2 \rightarrow Mg^{2+} + 2H^+ + 4e^-$	$E_0 = –1.114$ V
$MgH_2 \rightarrow Mg^+ + H_2 + e^-$	$E_0 = –2.304$ V
$MgH_2 \rightarrow Mg^+ + 2H^+ + 3e^-$	$E_0 = –0.768$ V
$MgH_2 \rightarrow Mg^{2+} + H_2 + 2e^-$	$E_0 = –2.186$ V
$MgH_2 + 2OH^- \rightarrow Mg(OH)_2 + 2H^+ + 4e^-$	$E_0 = –1.256$ V
$MgH_2 + 2OH^- \rightarrow Mg(OH)_2 + H_2 + 2e^-$	$E_0 = –2.512$ V
$MgH_2 + OH^- \rightarrow MgOH + 2H^+ + 3e^-$	$E_0 = –0.928$ V
$Mg + 2H^+ + 2e^- \rightarrow MgH_2$	$E_0 = + 0.177$V
$Mg + 2H_2O + 2e^- \rightarrow MgH_2 + 2OH^-$	$E_0 = + 0.177$ V
$Mg^{2+} + 2OH^- \rightarrow Mg(OH)_2$	$lg[Mg^{2+}] = 16.95–2pH$
$Mg + H_2 \rightarrow MgH_2$	$\Delta G = –8.17$ kcal/mol
$MgH_2 + 2H^+ \rightarrow Mg^{2+} + 2H_2$	$\Delta G = –92.42$ kcal/mol
$MgH_2 + 2H_2O \rightarrow Mg(OH)_2 + 2H_2$	$\Delta G = –296.074$ kcal/mol

As is seen, most of the electrochemical reactions have a negative standard equilibrium potential, which suggests that these reactions can be an anodic process of Mg corrosion in the electrochemical hydrogen process. In addition, in an aqueous environment, there are some reactions for water itself that can impact the corrosion of Mg [49]:

$H_2 \rightarrow 2H^+ + 2e^-$ $E_0 = 0$ V

$H^{2+} + 2OH^- \rightarrow 2H_2O + 2e^-$ $E_0 = -0.826$ V

In general, the above reactions may impact the corrosion of Mg by either contributing to the corrosion damage or affecting the corrosion process.

2.3 The surface film on magnesium and its alloys

If a metal spontaneously transform into its hydroxides or oxides, there is usually a hydroxide or oxide film covering the metal surface in a natural environment. Mg and its alloys are likely to be dissolved and oxidized in most of the natural environment, and the corrosion products will accumulate and form a surface film. In some cases, the surface film on Mg or its alloys may not be very protective; however, it can have a significant effect on other reactions taking place on the surface. It is of importance to understand the surface film to better explain the anodic and cathodic electrochemical reactions which may occur in the corrosion process of Mg and its alloys. The composition and microstructure of surface film on Mg vary depending on the composition of metallic substrate, formation conditions of the film and an environment [50]. Even though there have been many studies discussing the surface film on Mg and its alloy, the naturally formed surface film on pure Mg is still not well understood.

Generally, the surface film should mainly consist of $Mg(OH)_2$ and MgO [50]. $Mg(OH)_2$ is the main component in the film because it is more stable in an aqueous solution comparing to MgO, while in the dry atmospheric environment, MgO is the main component. In the natural environment, there is usually water vapour in the air, and a more stable hydrated oxide is formed in the surface film of Mg [51]. After the Mg sample is immersed into a solution, the original surface film first begins to react with water, and the main component of the outer layer of the film transforms to $Mg(OH)_2$. If there are chlorides in the solution, then they can react with the film and contribute to the formation of $5Mg(OH)_2 \cdot MgCl_2$ or $MgCl_2 \cdot 6H_2O$.

For magnesium alloy, the oxides or hydroxides of the alloying element are part of the surface film. For example, Chen *et al.* [52] found that Mg and Al hydroxides were two of the main compositions of the surface film on AZ91D magnesium alloy in an aqueous solution. Generally, Mg is more active and likely to react with oxygen and hydroxide than its alloying elements, such as Al, Zn and Mn. As a result, the main components of the surface film on magnesium alloys in the air are Mg oxides and hydroxides. The research result of Liu *et al*. proved that on some Mg-Al intermetallic, the Al/Mg ratio of the surface film is higher than the film formed on the substrate. One of the reasons may be the stronger affinity of Mg to oxygen and hydroxide compared with that of aluminum. One of the reasons why researchers still have difficulties understanding the surface film well is because its microstructure is not only a simple layer. Nordlien *et al.* [53] indicated that the surface film on Mg and its alloy is multi-layered. They believed that there was a thin and compact MgO film on top of the Mg substrate, and the thick and porous outer layer mainly consists of $Mg(OH)_2$.

Although the surface film of metallic Mg has a microstructural model, which assumes a compact inner layer and porous outer layer with that of Al, it is interesting that Mg surface film is not as protective as the Al surface film. In dry air at ambient temperature, the MgO surface film is too thin and ductile to cover the whole Mg surface, so it can only provide limited protection for Mg. However, if the film gets too thick at a high temperature, it still cannot offer good protection for the Mg because the film cracks due to the small Pilling-Bedworth ratio and becomes not protective [51]. In an aqueous solution, the $Mg(OH)_2$ film is harder to dissolve compared with the MgO film, but according to the theory, it is still unstable in an acidic, marine or weak alkaline solution environment. Besides, the film on the Mg surface cannot be compact or thick enough, so it can only provide limited protection for the substrate. The situation is quite different for Al substrate: there are Al_2O_3 and $Al(OH)_3$ in the surface film that is electrochemically stable between weak acidic and weak alkaline [50]. Therefore, the film of Al is quite stable and compact on the Al surface and can provide excellent protection for the substrate in many aqueous solutions, and this is the main reason why Mg and Al have different corrosion resistances in an aqueous solution.

Actually, in the air, there are always some oxides, such as MgO, formed on the Mg surface, and after the Mg sample is immersed into an aqueous solution, the surface film mainly consists of $Mg(OH)_2$. There are two possible explanation for this transformation: (1) direct hydration of MgO and (2) the dissolution of MgO as well as Mg and then the deposition of $Mg(OH)_2$. In the first case when the MgO is immersed into the solution, it is immediately hydrated, and the cubic MgO lattice is transformed into hexagonal $Mg(OH)_2$ whose volume is almost twice as that of MgO. This volume expansion is believed to give a rise to the porous microstructure of the $Mg(OH)_2$ surface film [54]. According to the second model, both the MgO and Mg substrate are dissolved, and that leads to the deposition of $Mg(OH)_2$ film on the surface because of its lower solubility in aqueous

solution. The deposited $Mg(OH)_2$ film is generally not compact and thus cannot provide enough protection for the Mg substrate. As a result, even if there is an inner MgO layer existing within the surface film in the aqueous solution, part of it transforms into porous $Mg(OH)_2$, and then the MgO film becomes discontinuous (see **Fig 2.2**). These areas are believed to be the defect place facilitating magnesium corrosion.

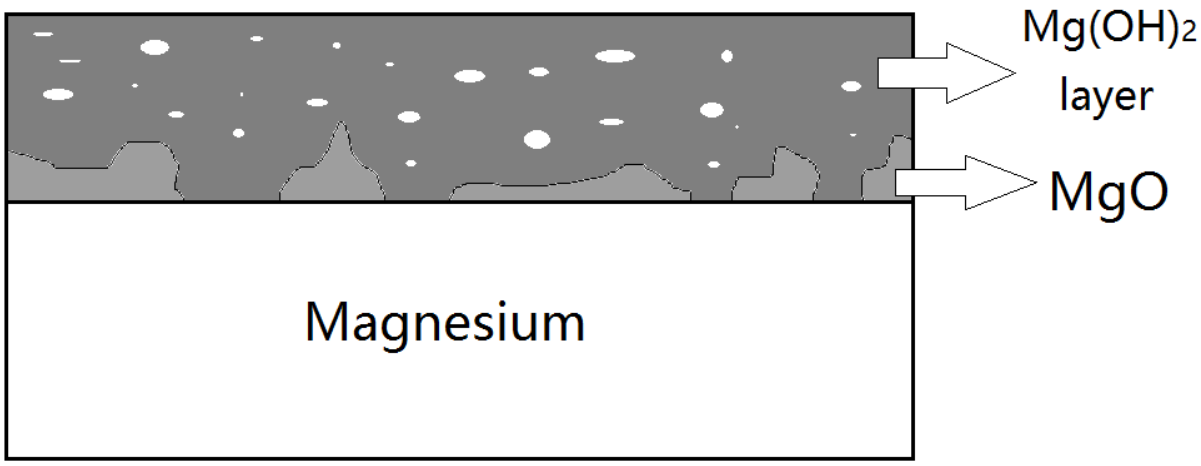

Figure 2.2. Schematic graph of the microstructure of Mg surface film

After the surface film breaks down, the corrosion of Mg initiates in these areas, and it is difficult for the surface film to recover by itself. As the hydrogen bubbles generating in the corrosion area the newly deposited $Mg(OH)_2$ is disturbed and cannot cover the surface. As a result, the formation rate of $Mg(OH)_2$ film cannot exceed the dissolution rate, and the corrosion cannot stop.

2.4 Corrosion protection of magnesium alloy

As described in the previous chapter, there is a spontaneously formed hydroxide layer on Mg and its alloys in moist air and aqueous solutions. This hydroxide layer is chemically stable in the alkaline environment but not stable in acidic or neutral solutions, especially when there exist

aggressive ions such as Cl^-, HCO_3^{2-} and SO_4^{2-}. Under those conditions, the $Mg(OH)_2$ film will dissolute, and thus the corrosion will continue at a high rate [56]. In order to protect the surface of Mg and its alloy, surface coating technique is used to prevent the aggressive ions from directly contacting with moisture and air. As a result, the anodic and cathodic electrochemical reactions do not occur or only occur at a low rate. In most cases, even partial blocking the cathodic reaction sites can significantly reduce the corrosion rate.

Some chemical and electrochemical methods like anodic treatments and cathodic treatments, as well as chrome pickling and chrome-free treatments, are widely used nowadays to develop the surface protection coatings for magnesium alloys to extend their service life. And other coating methods such as silane treatments, sol-gel and plasma vapour deposition were also used to improve the corrosion resistance of the surface of Mg and its alloys [56]. In the present study, the electrophoretic coating is mainly discussed.

2.4.1 Electrophoretic coating

Electrophoretic coating (E-coat) is a surface coating method and is also referred to as electrophoretic painting or electrodeposition. This coating technology is often applied for conductive materials like Mg to improve their corrosion resistance. This process is based on the electrophoretic motion of charged particles in an electrolyte towards an electrode under an applied electrical field. Depending on the setup process, electrodeposition can be divided into anodic and cathodic processes. In anodic electrodeposition process, the material to be coated functions as an anode and negatively charged particles in the electrolyte are driven towards the anode material by the electrical field and finally deposited on the material surface. While in the cathodic

electrodeposition process, the material to be coated functions as a cathode, which attracts positively charged particles under an applied electrical field.

Compared with other coating methods, the electrophoretic coating method has many outstanding advantages [56]. First, the coatings produced by the electrophoretic coating method are uniform and with low porosity, which means the coatings have excellent corrosion resistance. Second, this method can coat the complicated shape of surfaces because of its high throwing power as well as unique coating formation mechanisms. Third, this method has high efficiency and low cost for quantity production due to its high paint transfer efficiency (about 95%) and the high degree of automation and high throughput. Last, but not least, this method is environmentally friendly. Electrophoretic coating processes are mainly water-based and produce only a low amount of volatile organic compounds, and with no hazardous air pollutants. Heavy metals like lead have been eliminated from the bath electrolyte without reducing the corrosion resistance of the coatings. In conclusion, the above listed advantages have made the electrophoretic coating method an excellent surface protection choice for Mg and its alloys and also an important technique for the protection against corrosion in automotive industry.

The electrophoretic coating is done in three key steps [56]:

1. Pre-treatment of the material surface.

   Surface conditions of the materials, such as surface morphology, chemistry and contamination, have quite significant effects on the coating deposition, including the coating durability and its bonding strength. Therefore, to ensure good quality of the coatings, proper preparation of the material surface before the coating process is necessary.

There are several kinds of treatment methods for the material substrate including surface cleaning, which is quite significant in the coating industry [57], chemical etching, conversion coating, anodizing and plasma surface treatment. By using these methods, undesirable contamination on the surface will be removed.

2. Electrodeposition of the coating.

During a coating deposition process, a DC voltage is applied across the working electrode (substrate material), and the counter-electrode. Accompanied by the electrolysis of water, the charged particles in the coating electrolyte move towards electrodes with opposite charges. Due to the water electrolysis, oxygen gas is produced on the anode, and hydrogen gas is produced on the cathode. Then the hydrogen ion equilibrium in the water surrounding the electrodes is disturbed by the evolution of these gases. This leads to a pH change that de-stabilizes the electrolyte compositions and ions deposit on the magnesium alloy electrode.

The chemistry of the coating electrolyte and the deposition parameters, including temperature, applied voltage and coating time, are all primary factors that have a significant effect on the coating quality [56].

3. Post-rinse and baking.

After coating deposition, the coated material is usually rinsed to clean its surface. After the rising process, the coated film of the materials is to be cured by placing it in an oven. During the baking process, the coated film becomes harder and more resistant to corrosions. What's more, the coating film becomes denser and more continuous after the baking

process because of the filling of gas pores which are formed in the deposition procedure. Usually, the baking temperature is set in the range of 82-177 ℃ (180-350 ℉) [56].

In conclusion, the electrophoretic coating is a low-cost and simple coating method to protect the Mg and its alloys. However, the coating schemes nowadays are complicated multi-layer systems, which include many different technologies of manufacturing. In order to achieve the optimum final results, the coating process has to be conducted carefully, and its processing has to be appropriately controlled.

Even though the electrophoretic coating technology is well established now and has been commercialized for mass production for several decades, there are more demands for further improvements of corrosion resistance, productivity, cost of manufacturing and the processing that is more friendly to the environment. Compared with steels and aluminum alloys, magnesium alloys are relatively new for engineering applications, and they need more improvements in terms of mass production [56]. The significant performance required to be improved includes better corrosion resistance and durability, better coating adhesion to the material surface, control of colour, as well as better chipping resistance. Some of them need the modification of the electrolyte components to have improved coating chemistry while others may require changes of the pre-treatment method or optimizing the coating parameters.

Besides, the cost reduction is always a critical demand for electrophoretic coating manufacturing. Several areas of processing are focused on cost reduction, and on some crucial aspect of optimizing and reducing the baking temperature and time. The baking is the process that consumes a lot of energy. Another promising coating method is the “electroless” organic coating, which has potential to improve the productivity and to reduce energy consumption.

2.4.2 Previous research on MgO coating on magnesium alloy

Lei *et al*. [14] have investigated the corrosion resistance of MgO coating electrodeposited on magnesium alloy by anodization in 6 M KOH solution. $Mg(OH)_2$ coating is produced by anodization in 10 M KOH solution and the authors observed MgO conversion from $Mg(OH)_2$ by calcination in air at 450°C. The evolution of morphology and components of the anodic surface film formed on magnesium alloy is investigated in this research. The rate of nucleation and growth of coatings was enhanced in 10 M KOH, and these coatings had improved corrosion resistance on the Mg substrate relative to the bare metal. This improvement was related to higher OH^- concentration in 10 M KOH solution that helped with faster nucleation and growth of $Mg(OH)_2$ on the surface of the electrode during the electrodeposition process, which could be converted to MgO coating through heat treatment. Cai *et al*. [15] have investigated the anodic oxidation of Mg in KOH by the alternative current impedimetric method. Anodization of the substrate initiated both active dissolution and passivation. The charge transfer process controlled Mg dissolution at the active region while $Mg(OH)_2$ deposition was the dominant reaction at the passive region and the oxidation region. As indicated by the authors, the primary oxidation steps were preceded by a secondary oxidation reaction where Mg spontaneously oxidized to MgO and this process was controlled by charge transfer and diffusion of water. The authors explained the Mg electrochemistry utilizing anodic polarization in 6 M KOH solution at different scan rates and by recording impedance curves at varying amplitudes Li *et al*. [60] investigated the effects of electrolytic coating parameters on corrosion resistance of MgO coating on magnesium alloy. The as-coating, which was $Mg(OH)_2$, was carried out in 0.1 M $Mg(NO_3)_2.6H_2O$ aqueous solution and later transformed to MgO by heat treatment at 350°C. The author used grazing angle X-ray diffraction and scanning electron microscope (SEM) to investigate the phase structure and surface

morphology. Also, corrosion resistance of the coated magnesium alloy samples was analyzed by conducting polarization curves and immersion tests. The result showed that a more negative applied potential produced more OH^- ions and enhanced the migration of Mg^{2+}, which caused a higher formation rate of $Mg(OH)_2$ on the sample and the (001) preferred orientation. The increasing deposition time within the starting 40 minutes led to the increase of coatings, which could be supported by the weight gain result, and the coating increasing rate slowed down after one hour because of the precipitation of $Mg(OH)_2$ in the solution. According to the final results, the optimum MgO coating quality could be obtained by deposited at -1.8 V (Ag/AgCl) for 40 minutes and calcined at 400°C for one hour as the protective coating was denser and more uniform. The comparison of surface morphology of bare magnesium alloy sample and the MgO coated sample showed that the coated sample had excellent anti-corrosion performance. This conclusion could also be supported by the reduction of corrosion current density from 99.5 down to 0.2 $\mu A/cm^2$ as well as the enlarged passivation region between -1.52 V and -1.25 V (Ag/AgCl) in 3.5 wt% NaCl solution, compared to the bare magnesium alloy. However, there still existed a problem for the bonding strength, and it should be improved to reach the minimum requirement, 35MPa from the now 10 MPa strength for orthopedic implants use. Apart from electrodeposition, recent development in coating technology has also seen significant progress in micro-arc oxidation as a plasma anodizing technique for magnesium alloys [16,17]. The electrolytic deposition of MgO coatings on nickel superalloy in our laboratory has also been reported [18], but the effect of heat treatment on the coating barrier performance of coating still needs to be investigated.

CHAPTER THREE

MATERIALS AND METHODOLOGY

3.1 Reagents and materials

The following reagents were utilized as corrodents in this study: sodium hydroxide ($\geq$98%), potassium hydroxide ($\geq$85%), sodium chloride ($\geq$99.5%), potassium chloride ($\geq$99.0%), sulphuric acid (99.99%), hydrochloric acid (>37%); all purchased from Sigma Aldrich. All reagents were analytical grade, so they were used without further purification. For the corrosion test alone, one-molar (1 M) concentration of these reagents was utilized, prepared using deionized water (conductivity $<$ 0.3 μS/cm).

3.2 Material and material preparation

The metal substrate used in this study is ZX10 magnesium alloy with the following chemical composition: Zn (1 %), Ca (0.2 %), Nd (0.5 %), Si (0.01 %), Mn (0.01 %), Fe (0.02 %), with magnesium making up the balance. Several coupons (20 mm × 20 mm × 4 mm) were mechanically cut out from a big plate and polished using SiC papers, starting with 1200 to 4000 grit sizes. The abrasion and following polishing procedure were conducted on LaboPol-20 manual polishing machine, as shown in **Figure A.1** and the standard operating procedure is presented in Appendix A. Pure ethyl alcohol was used as the washing liquid throughout this physical abrasion procedure before deploying polishing with MD/DP-Mol (3μm) and then diamond suspension (1 μm) on MD Nap. The last polishing step involved a gentle abrasion using OPS on MD-Chem cloth until a mirror surface was achieved. The OPS solution composed of a mixture of ethylene glycol and 99%

ethanol in equal proportions. The abraded metal substrates were then dried in warm air and stored in a desiccator before use.

3.3 Corrosion tests

The general corrosion behaviours of ZX10 magnesium alloy substrates in each media were investigated by means of weight loss technique. Impedance spectra for respective substrates were collected at open circuit potential (E_{OC}) with a 10-mV sine perturbation using electrochemical impedance spectroscopy (EIS). In the potentiostatic mode, data were collected from 10^{-2} to 10^{5} Hz for Mg substrates exposed at 1-cm^2 area. Potentiodynamic polarization technique also complemented the EIS; polarization curves for each metallic substrate in the potential range from −0.5 V to the final potential of 0.5 V vs. (Ag/AgCl) with a scan rate of 0.5 mV/s. The EChem analyst software (Gamry Instruments) was used to analyze the electrochemical data. These electrochemical tests were conducted using a potentiostat/Galvanostat/ZRA (Interface 1000, Gamry Instruments) with each substrate serving as working electrodes, coupled to paint cells. These cells were connected to the reference (Ag/AgCl (sat. KCl)) and counter (graphite rod) electrodes, exposed to corrodents at room temperature. The corrosion behaviour of magnesium alloy was also investigated through the weight loss technique after a 2-week complete immersion within each corrodent. This immersion test was aimed at computing the corrosion rate of the Mg substrates. The corrosion rate was measured by taking the weight differences before and after exposure of these coupons within the duration of the test [21]. The presented results in this work are averages of triplicate measurements. Before weighing, each metallic coupon was washed with water and dried in the warm air; weighing was accomplished with the aid of an analytical balance (Sartorius, Germany; sensitivity ±0.001 mg). The impact of aqueous corrosion on the

microstructure of the Mg substrate in each corrodent after a two-week exposure period was probed by scanning electron microscopy (SEM; Hitachi SU6600 scanning electron microscope, as shown in **Figure B.2**). Evidence of adhesion of corrosion products on the surface of Mg substrate was also examined using SEM and X-Ray Diffraction (XRD) technique. XRD analysis was conducted using an Apex2 Kappa CCD 4-Circle Kappa FR540C diffractometer (Brüker AXS). Gradual corrosion-induced changes at the grain boundaries within the Mg microstructure and these changes were also probed at room temperature using electron backscatter diffraction technique (EBSD) after in-depth microstructural and crystallographic texture analyses. Analyses were accomplished with EBSD detector coupled to the SEM. The EBSD scans were recorded using an accelerating voltage of 30 kV. Electron diffraction patterns were collected using Oxford Instrument's AZTEC 2.0 software using a step size of 0.14 μm, and post-processed with the Channel 5 software. Also, grain boundaries with misorientation angles below 15 degrees were categorized as low angle grain boundaries while angles above 15 degrees were considered as high angle grain boundaries.

3.4 MgO coating preparation procedure on Mg substrate

The ZX10 magnesium alloy test substrate deployed in this work were cut into 2.5 cm × 2.5 cm × 0.5 cm sized coupons and polished with diamond paste and alumina suspension. The coupons were then cleaned with isopropanol (100%, Sigma Aldrich) in an ultrasonic bath, dried in warm pressurized air and stored in a desiccator before electrodeposition. Coating deposition was conducted electrochemically in a 0.5 M magnesium nitrate hexahydrate (100%, Sigma Aldrich) electrolyte bath in a water-ethanol (50:50) mixture. The magnesium substrate and graphite (in a sealed Teflon jacket) represented the cathode and anode electrodes, both connected to a current-source rectifier (EG&G Instruments Potentiostat). The electrodeposition of coating on the

magnesium alloy substrate was carried out by applying 20 mA/cm^2 current density to the cathode for 60 minutes at room temperature without stirring the electrolytic bath. Each coated substrate was then dried at room temperature for another 60-min duration before weighing. In order to transform the $Mg(OH)_2$ coating to the MgO coating, the specimens were subsequently calcinated at different temperatures between 50, 250 and 500°C and the influence of different calcination temperature on corrosion resistance of coatings was also investigated. These temperatures are chosen for the calcination because the dehydration of $Mg(OH)_2$ to form MgO occurs in the temperature range of 290 and 410°C [66]. The calcination procedure was conducted under the air atmosphere in a muffle furnace ceramic tubes for 30 minutes.

3.5 Characterization of MgO coatings

After the calcination, the phase composition and crystallization of each coating were determined by X-ray techniques. X-ray diffraction (XRD) spectra of the calcinated coatings were recorded at room temperature using a Bruker D8 Discover XRD Diffractometer operating with Cu-K_α radiation. X-ray photoelectron spectroscopy (XPS, Kratos AXIS Supra X-ray Photoelectron) was used as a complementary technique to evaluate the composition of the coating systems, using a monochromatic Al-K_α X-ray source. XPS data collection was accomplished at a 90° photoelectron take-off angle relative to the sample surface plane on relatively small spot sizes (in a few hundred microns). The XPS spectra were later presented as wide-scan. These are also accompanied by high-resolution plots for specific elements using deconvolution non-linear least squares algorithm with Gaussian–Lorentzian combination analyzed with a CasaXPS software (version 2.3.19). The XPS technique is principally based on gathering ejected electrons from atoms within test samples that are irradiated with X rays. It provides unique information about the chemical makeup of

samples. There may be issues with a penetration depth of X rays, but this technique is nondestructive and samples are not chemically or structurally changed. The microstructures of calcinated MgO coating deposits at different temperatures were also examined using scanning electron microscopy (a Hitachi SU6600 SEM, show in **Figure B.2**) at 20 kV acceleration voltage. The microhardness of all coated specimens was measured using dynamic hardness tester (Micro-Combi, CSM Instruments) using a pyramid indenter under an indention load of 100 gf and 10-second dwell time. The Vickers hardness (HV) values were then computed and presented as average values of three measurements.

3.6 Evaluation of the corrosion resistance of calcinated MgO coatings on magnesium substrates

Electrochemical impedance spectroscopy (EIS) was utilized in investigating the corrosion resistance of calcinated MgO coatings on Mg substrates in 3.5 wt% NaCl with the aid of a Potentiostat (Interface 1000, Gamry Instruments). This test was conducted by applying a small amplitude perturbation, 10 mV peak to peak at open circuit potential (E_{oc}) between 0.01 and 100 kHz. The E_{oc} is representing the equilibrium potential within the test solutions with no external electric current flow. Tafel curves of respective coatings were also collected by a potentio-dynamic polarization experiment. This complementary direct-current test was conducted by applying a potential range of $\pm$0.25 V vs E_{oc} at a scan rate of 1 mV/s. The electrical potentials were measured relative to the Ag/AgCl (sat. KCl) reference electrode (E_{ref}) connected to the potentiostat with graphite counter and coated magnesium working electrodes. An area of one square centimeter was defined on the working electrodes with an aid of the electrochemical mask (Gamry, US) for each test.

CHAPTER FOUR

RESULTS AND DISCUSSION

4.1 Degradation behaviour of bare magnesium alloys

4.1.1 Electrochemical analysis

The EIS measurements were conducted with a range of signals that has relatively no effect on test samples, hence, no inherent electrochemical-induced damage of the metallic substrate [29]. The corrosion behaviour of Mg substrates was monitored after applying small sinusoidal perturbations while measuring the corrosion current density. The different aggressive media with varying pH values were chosen for this study to account for localized corrosion behaviour accompanying charge transfer. Buildup of passive Mg oxide films led to gradual resistance to charge transfer processes. **Figure 4.1 (a-c)** depicts the Nyquist plots for Mg substrates in corrosive media. These impedance spectra possess single capacitive loops at high frequencies and inductive loops at low frequencies. Normally, nanocrystallization increases the thickness of passive film on Mg substrates with rare elements. In this work, the grade of magnesium alloy studied has none. However, the passive hydroxide films become the prominent corrosion product film on the Mg substrate. These films resist the dissolution of Mg material but did not necessarily inhibits its corrosion since the substrates are completely immersed within corrodent [30]. The high-frequency capacitive loops are mainly controlled by inherent interfacial charge transfer processes while the low-frequency inductive loops may be related to the dissolution of poorly formed or not well adsorbed passive films on the Mg electrodes. The curves with wider diameters are obtained for

metal systems with enhanced resistance to corrosion and Mg appears to corrode more in the acidic media with no apparent changes in the alkalis or water.

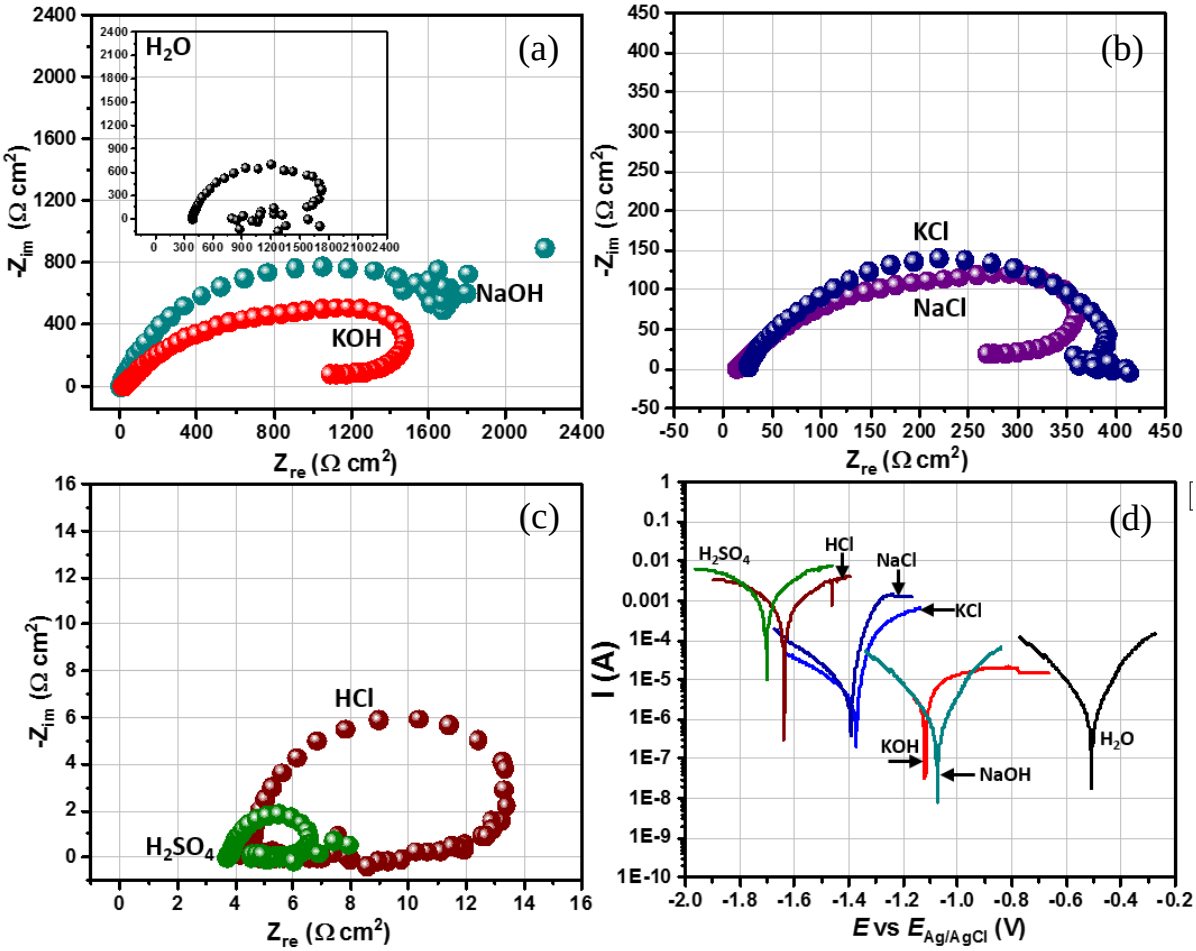

Figure 4.1. (a)-(c) Electrochemical Nyquist and (d) Tafel polarization curves for magnesium alloy in different corrosive media.

After fitting the experimental impedance data into an electrochemical circuit model [$R_{soln}(Q(R_{ct}(R_L L)))$], as shown in **Figure 4.2** and the parameters in **Table 4.1** were collected. Relative to pure water, the trend of charge transfer resistance (R_{ct}) values for Mg within other electrolytes is consistent with intense corrosion, especially for the acids. The R_{ct} values for Mg in NaOH, KOH and water suggest no corrosion due to the presence of undissolved passive oxide films. As with the resistance, the electrochemical phases in the impedance curves depicted in

Figure 4.1 are also represented by some capacitance component. This capacitance component is a constant phase element (Y_o, Q) that accounts for depressions on impedance curves resulting from lack of surface homogeneity and distortions on the double-layer [32]. Q is equivalent to $Y^{-1}(j\omega)^{-n}$ and Y is the magnitude of Q and n is an empirical number ($0 \leq n \leq 1$). j is an imaginary constant $\sqrt{-1}$ and ω is angular frequency (equals to $2\pi f$), where f is the frequency in Hz. More resistive metal systems have lower value of Q_{dl}, and this denotes higher thickness of electrical double layer resulting in less corrosion [35]. In this work, the order of decreasing Q_{dl} values is Mg in water < KOH < NaOH < KCl < NaCl < H_2SO_4 < HCl. Other electrochemical parameters (inductor (L) and inductive resistance (R_L)) representing the inductive Nyquist loop are also presented in Table 4.1.1.

Table 4.1. Electrochemical parameters for magnesium substrates exposed to various corrosive electrolytes at room temperature

Mg Substrate in:	Electrochemical impedance spectroscopy					Potentiodynamic polarization technique			
	R_{soln} (Ω cm^2)	R_{ct} (Ω cm^2)	Q_{dl}, Y_o (μF cm^{-2} s$^{-(1-\alpha c)}$)	R_L (Ω cm^2)	L (H cm^2)	-E_{corr} vs Ref (V)	j_{corr} (μA/cm^2)	β_a (mV/dec)	β_c (mV/dec)
H_2O	5.1	1815.8	4.0	525.9	0.5	0.50	1.0	38.2	72.1
NaOH	8.6	1650.2	10.6	415.4	1.5	1.10	1.1	79.0	109.3
KOH	9.2	1100.7	16.9	263.2	6.3	1.15	1.0	59.9	92.1
NaCl	15.6	320.1	126.8	129.9	6.9	1.40	62.5	99.2	154.2
KCl	21.5	420.6	108.1	149.1	5.2	1.39	10.0	109.4	141.9
HCl	10.3	13.4	1400.1	102.4	2.9	1.65	100.9	68.8	90.0
H_2SO_4	12.5	5.1	2241.4	89.7	1.2	1.70	902.8	79.9	83.9

Goodness of Fit (χ^2) values were less than 10^{-4}

Electrochemical impedance spectroscopy is also complemented by potentiodynamic polarization technique. The latter technique probes the rate of electron transfer on metal substrates within corrosive solutions. In this work, polarization curves for Mg substrate in each corrodent were collected in potential range between −0.5 and 0.5 V vs (Ag/AgCl) at a 0.5 mV/s scan rate (as presented in **Figure 4.1d**). After performing Tafel fitting, electrochemical parameters [(anodic (β_a)

and cathodic Tafel (β_c) slopes, corrosion current density (j_{corr}) and corrosion potential (E_{corr})] are presented in Table 4.1.1. As expected, the values of j_{corr} are reduced for more resistive systems, and this is consistent with corrosion inhibition initiated by the coverage of Mg surface with absorbed passive films, especially in the alkali solutions as well as water. The order of decreasing j_{corr} is Mg in water < KOH < NaOH < KCl < NaCl < H_2SO_4 < HCl. The least observed magnitude of j_{corr} (1.0 µA cm^{-2}) was recorded for Mg in water while Mg corroded most in NaCl for the salt (62.5 µA cm^{-2}) and H_2SO_4 (902.8 µA cm^{-2}) in the acidic solutions. A cursory view at these polarization curves also reveals steady shifts toward more negative values for Mg substrates in more corrosive solutions. An approximately 120 mV vs E_{ref} shift in E_{corr} for Mg in water and HCl was recorded while approximately -138 and -139 mV vs E_{ref} were observed for Mg substrate in NaCl and KCl, respectively.

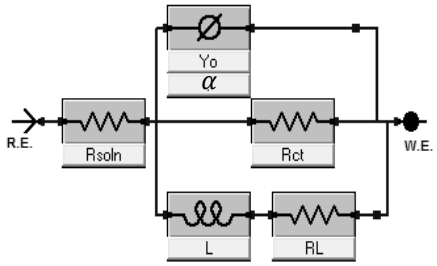

Figure 4.2. The equivalent circuit model [$R_{soln}(Q(R_{ct}(R_L L)))$] used in fitting the experimental impedance data for Mg substrates exposed to the corrosion media. This circuit was modeled with resistive (solution resistance (R_{soln}), charge transfer resistance (R_{ct}) and inductive resistance (R_L)), capacitive (double layer capacitance (Q_{dl})) and inductive (L) components.

4.1.2 Weight loss measurement

The variation in values of weight loss (Δw) and corrosion rates (v) of Mg substrates upon exposure to these corrosive electrolytes are presented in **Figure 4.3**. It is clear that the substrate lost most of

its mass within the two corrosive acidic media compared to the chloride-rich salt solutions; this is indicative of severe corrosion phenomenon at low pH. The average weight losses for Mg coupons in the salt and acid media are 1.6 and 3.4 g/cm^2, respectively. The trend of results also confirms no significant reduction in the mass for Mg substrates within the alkali and water due to reduced reactivity and the presence of undissolved primary oxide passive films. Two weeks was enough time to demonstrate that even when this Mg passivated, the rate of localized breakdown of these passive films still led to accelerated dissolution of the metal.

The magnitudes of corrosion rate (v), in mpy (mils per year) were computed for Mg substrates exposed to all the solutions using this equation [67]:

$$\boldsymbol{v\ (mpy) = (3.45 \times 10^6 \times \Delta w)/\rho AT.}$$

In this Equation, ρ is the density of Mg (g/cm^3), A is the average surface area (cm^2) of the Mg specimen while t (h) denotes the time of exposure of the metallic substrates to the corrodent. The weight loss experiments were conducted for all Mg substrates at room temperature. Values of v for each coupon relates to their cross-sectional area, density and duration of exposure to respective corrosive media, computed from triplicate Δw measurements. The metal substrates corroded more in the acid solutions due to the spontaneous reactivity of Mg in solutions of low pH. The whole mass completely dissolved within the first three days of exposure to HCl and H_2SO_4 therefore the presented values of corrosion rate were computed after 3 days (only for Mg substrates in the acid solutions). The magnitudes of corrosion rate went up to 19678 and 26723 mpy for Mg substrate in 1 M HCl and H_2SO_4, respectively. After two weeks, the Mg substrates corroded at the rate of 2193 and 2515 mpy for KCl and NaCl, respectively. Mg neither reacted in the aqueous alkaline nor in

doubly distilled water. Corrosion rates of the substrates within these media were recorded as 0, 0.3 and 1.5 mpy, for water, NaOH and KOH, respectively.

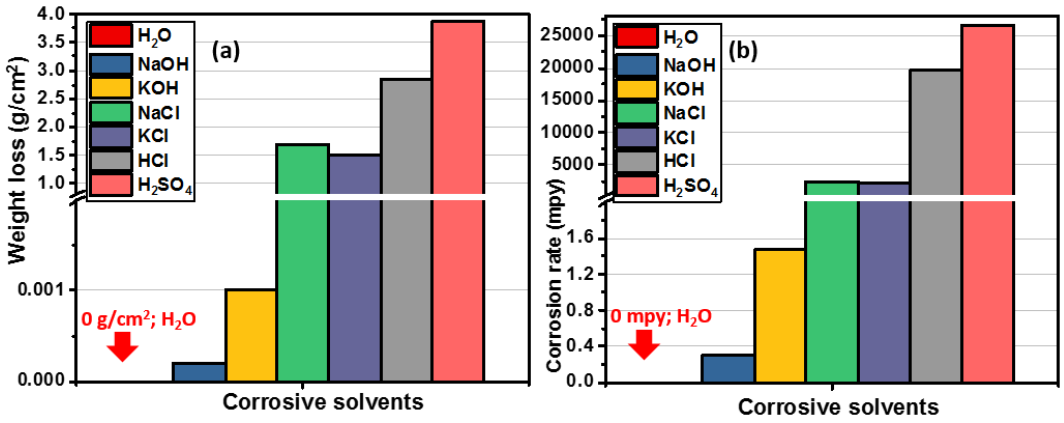

Figure 4.3. Variation in values of weight loss and corrosion rate of magnesium coupons exposed to different corrodents at room temperature (magnesium showed no significant reaction in the aqueous alkaline nor in doubly distilled water).

4.1.3 Surface analytical evaluation

Figure 4.4 represents photographs showing the appearances of the Mg coupons exposed to different corrodents at room temperature. The extent of Mg corrosion is linked with its reactivity in these media at different exposure times. In all, Mg substrates significantly corroded at low pH due to its spontaneous reaction in these acid solutions. The metal had completely dissolved in sulphuric acid while significant mass loss could be observed for Mg in HCl within 72 h. Here, the rate of dissolution of metal mass exceeds its passivation ability as more primary oxide films are dissolved within the media. In the salt media, the rate of Mg corrosion reduces due to the stability of oxide films formed during the test. The dissolution of passive hydroxide/oxide and chloride films dominates the mechanism of Mg corrosion as the metal mass depletes in NaCl and KCl. Mg show no reactivity in the aqueous alkaline solutions and in doubly distilled water due to passivation;

the presence of these layers further improved corrosion resistance as less metallic mass degrades. For Jiang *et al.* [36], claim that the reaction of Mg in corrosive chloride solutions leads to the formation of different Mg salts accompanied by hydrogen gas. Normally, magnesium hydroxide ($Mg(OH)_2$) may readily degrade in the presence of sulphate or chloride ions to form magnesium chloride ($MgCl_2$). This adhering corrosion products are also loosely attached films that may detach leading to percolating ionic pathways and subsequent degradation of Mg substrate [37].

Figure 4.5 depicts the SEM micrographs of magnesium alloy coupons exposed to different corrodents after 3 days. The adhesion of passive films/corrosion products on these metal surfaces gives an idea of the extent of Mg resistance to aqueous corrosion. Since magnesium corrosion was still at the early stage, these metal surfaces were covered with few passive films. Fine crystalline $Mg(OH)_2$ grains grew at the solid/liquid interface for all substrates. These corrosive ions continued to penetrate through micro-holes within the $Mg(OH)_2$ films. At the metal surface, these ions reacted with the magnesium alloy substrate leading to surface pits. Except for the alkaline media and water, magnesium alloy corroded severely in all media, especially in the acid and saline media. The specimen substrates did not react much in the aqueous alkaline solutions and the observed aggregates are passive films mixed with crystals of the solvents that were formed after mild-heat drying. These fine crystalline grains appeared as aggregates of rather thick $Mg(OH)_2$ film for the specimen substrates in highly corrosive media [36]. In this work, I also observed that subsequent heat treatment must have induced the formation of MgO. This could be the reason for the turbid flakes appearing on the surface of Mg in the saline media. According to Hsu *et al.* [38], these passive oxide films isolate the underlying metal surface from the corrosive ions and can be a few nanometers in thickness. The removal of these films due to localized dissolution upon prolonged exposure only leads to eventual acceleration of metal corrosion at defined pitting sites.

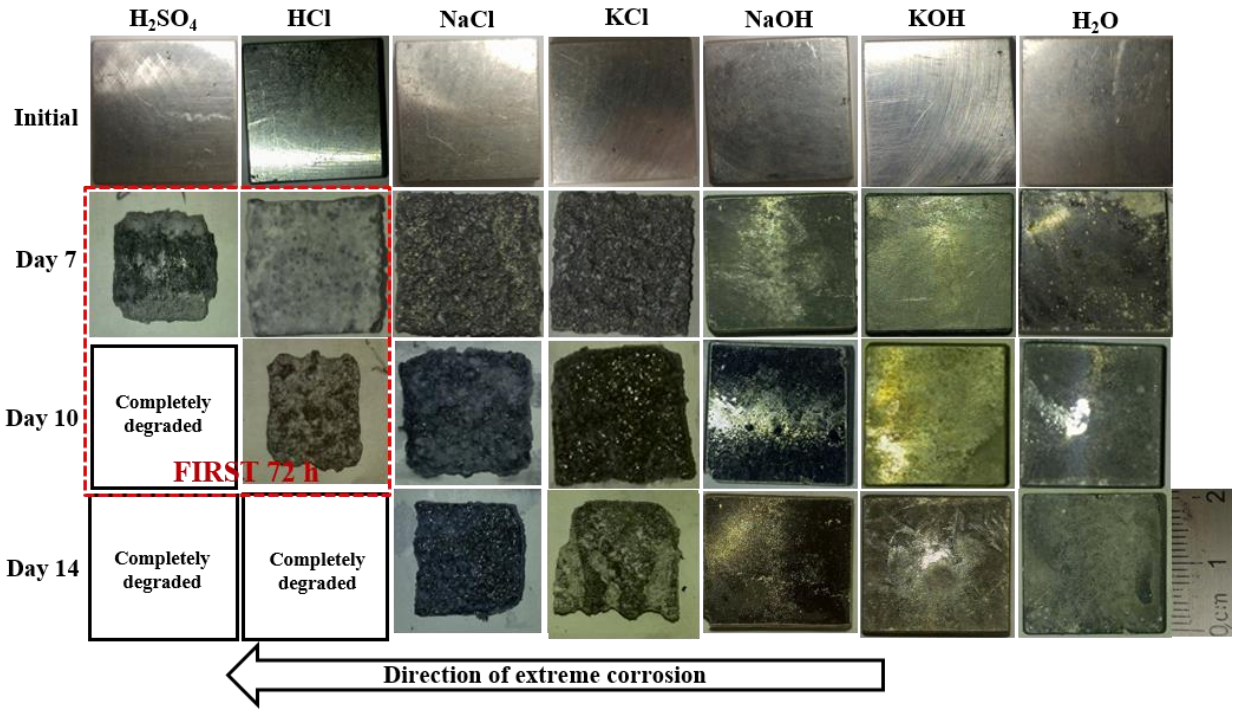

Figure 4.4. Appearances of the Mg coupons exposed to different corrodents (the extent of corrosion of Mg can be linked with its reactivity in these media at varying exposure periods).

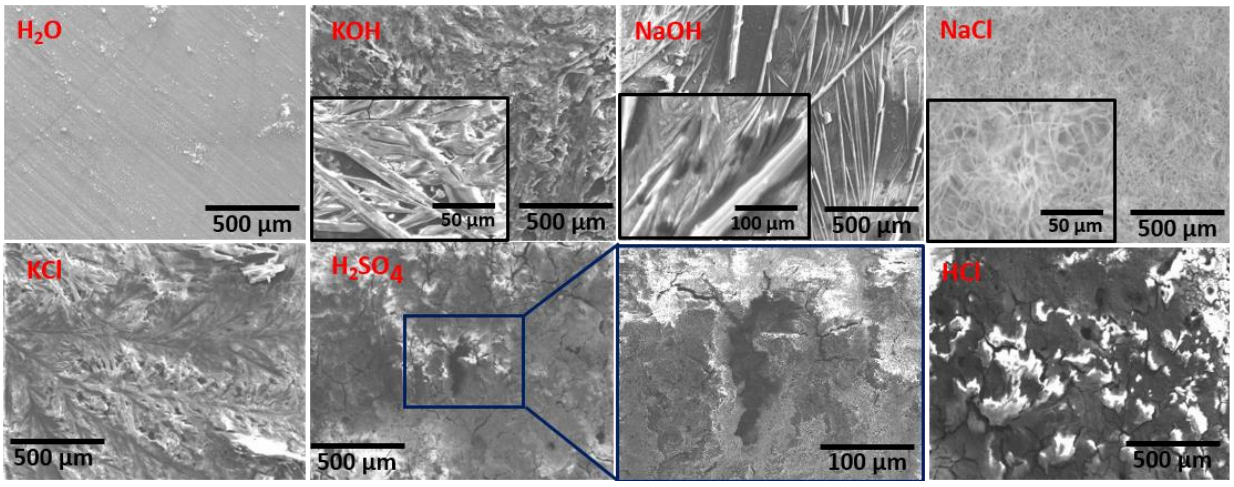

Figure 4.5. SEM micrographs of Mg coupons showing adsorbed passive films/corrosion products after exposures to different corrosive media for 72 hours.

4.1.4 Corrosion at the grain boundary

In a clinical study involving Mg implant [39], authors demonstrated that this metal completely dissolves within few weeks (about 6 weeks) of installation. This confirms that even when Mg readily forms passive MgO and $Mg(OH)_2$ films, these adhering protective layers do not sufficiently protect the metal substrate. However, these passive layers do not always evenly form on the metal substrate as presented in **Figure 4.5** To account for this assertion, changes at the grain boundaries during the corrosion of Mg substrates in chloride-enriched simulated body fluid at room temperature are further monitored. **Figure 4.6** shows the grain boundaries within the Mg substrate from inverse pole figure (IPF) map investigated for this sample. The grain orientations are color-coded (**Figure 4.6a**) and the IPF triangle (**Figure 4.6b**) shows more grain oriented near {0001}. The grain distribution of this alloy is presented in **Figure 4.6c** (with an average grain size of 116 μm) while the average grain size was measured as the average of the diameter of all the grains in the EBSD map. In this study, mildly-etched Mg substrates were marked by indentation before monitoring possible changes at the grain boundaries during the early stages of Mg corrosion. This was done after the EBSD analysis. Changes within this metallic coupon were observed periodically within the first three hours before total passivation. **Figure 4.7** shows changes in the surface morphologies of the Mg substrate at different durations; the grain boundaries are still conspicuous after an hour of exposure to the corrosive media. However, the accumulation of corrosion products over the grain boundaries are observed at end of the second hour. Since these sites are thermodynamically more active, $Mg(OH)_2$ films within these regions further reduces corrosion attack [40, 41]. The accumulation of passive films/corrosion product aggregates over the boundaries continues after the third hour until Mg surface is completely covered. At this stage there are no pits, except few thin and uneven passive films of corrosion products that are also

susceptible to exfoliation due to the presence of micro-cracks. These grain boundaries and α and β phases within the Mg matrix play a major role in the passivation behaviour over a wide range of pH. The β phase is directly related to alloying content, grain size and the grain distribution pattern within the matrix [40]. **Figure 4.8** shows the SEM and EDS micrographs of Mg/passive film interface after corrosion test. While the bare metal shows elements consistent with the bare alloy content, the passive layer is predominantly $MgO/Mg(OH)_2$ and $MgCl_2$ film. On these films, ionic transport though vacancies is influenced by the non-stoichiometric nature of the oxide, however, fast ion transports may occur at metal/oxide interfaces.

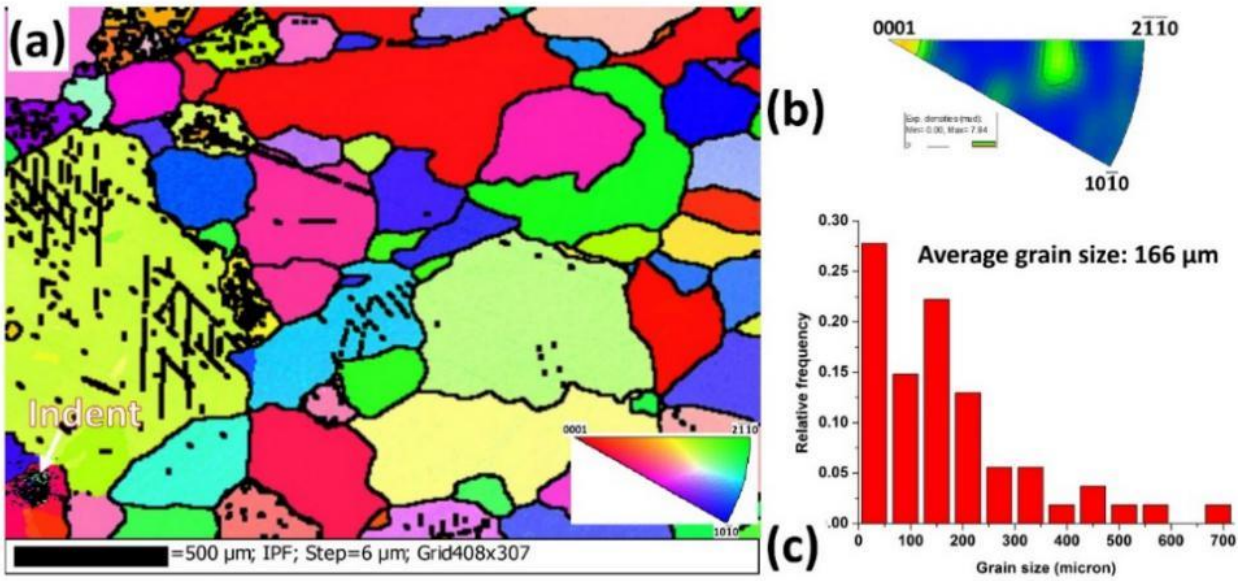

Figure 4.6. EBSD (a) IPF map, (b) IPF triangle and (c) grain size distribution of the sample before corrosion

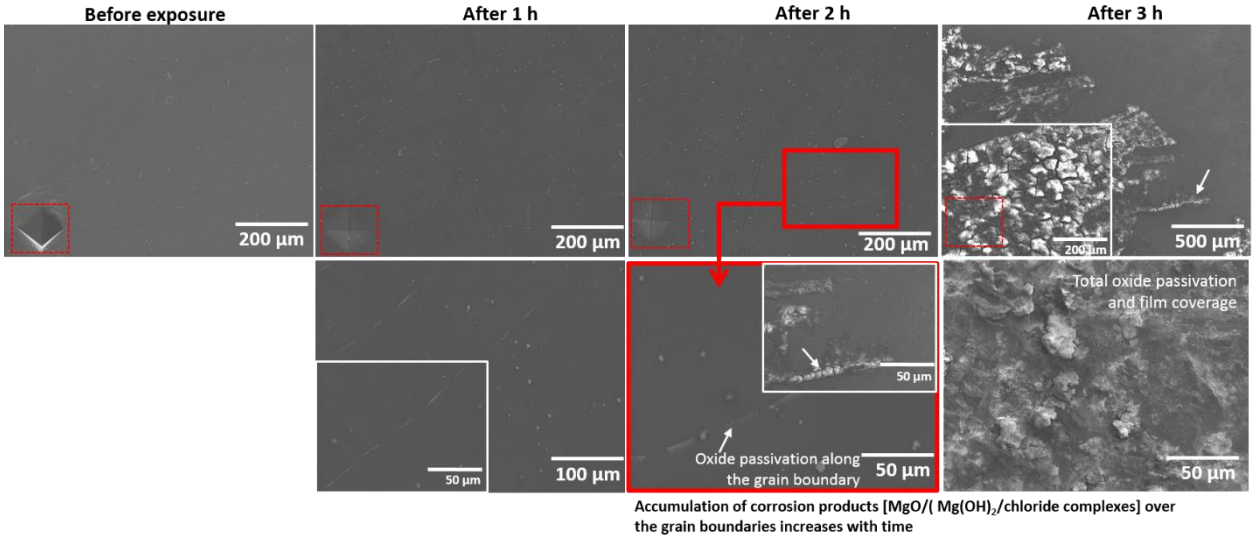

Figure 4.7. SEM micrographs of Mg substrate exposed to chloride-enriched simulated bodily fluid showing changes at the grain boundaries during the early stages of corrosion.

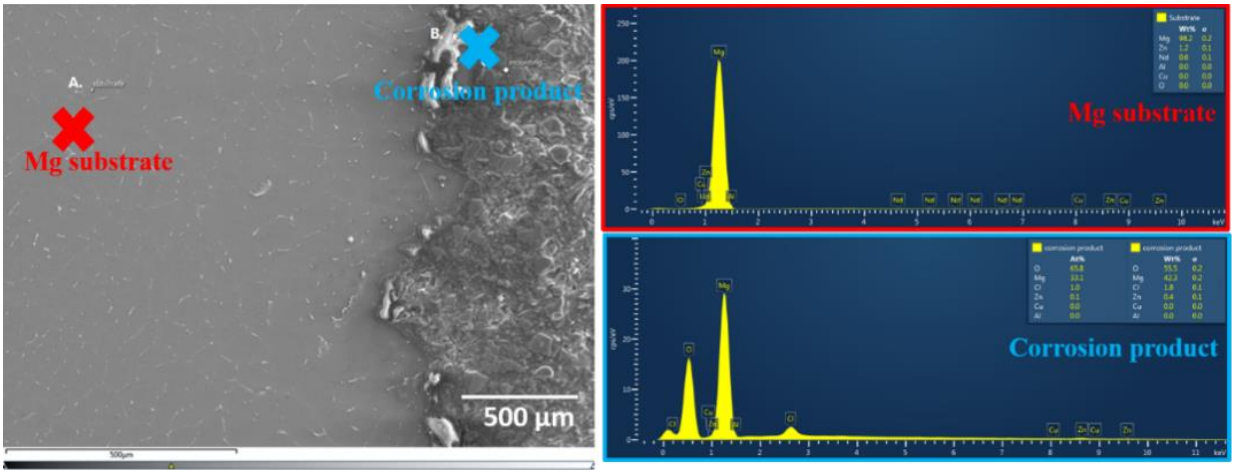

Figure 4.8. SEM and EDS micrographs of Mg/passive film interface after corrosion of the metal in chloride-enriched simulated bodily fluid.

4.1.5 Analysis of adhering corrosion products

The chemical composition of the corrosion products in **Figure 4.5** was also analyzed using XRD technique and results are presented as XRD spectra in **Figure 4.9**. As depicted on these spectra,

the adhering corrosion products/passive films on Mg coupons shows peaks corresponding to amorphous structures of $Mg(OH)_2$ and MgO exposed to different corrodents. These adhering products exhibit strong Mg peaks and other product (e.g. $MgSO_4$ and $MgCl_2$) peaks of different intensities. The $Mg(OH)_2$ films reveal intensities at (001), (101), (110) and (201) while MgO peaks are weaker at (111), (200) and (220). The chemical composition of these passivated surfaces describes the dissolution mechanism of the active/passive transition of Mg metal within these corrosive media. The thicknesses of the oxide layer of these passivated Mg surfaces may determine the diffusion rate of corrosive ions through them, though preferential ion transport may also occur at the grain boundaries. These oxides gradually grew over time, isolating the metallic surface. However, when the rate of degradation exceeds passivation, extreme corrosion is imminent. Oxidation reaction tends occurs at the metal/oxide interface while oxygen reduction occurs at the outer oxide surface [38]; more authors have also reported related assertions [42, 50, 58-59].

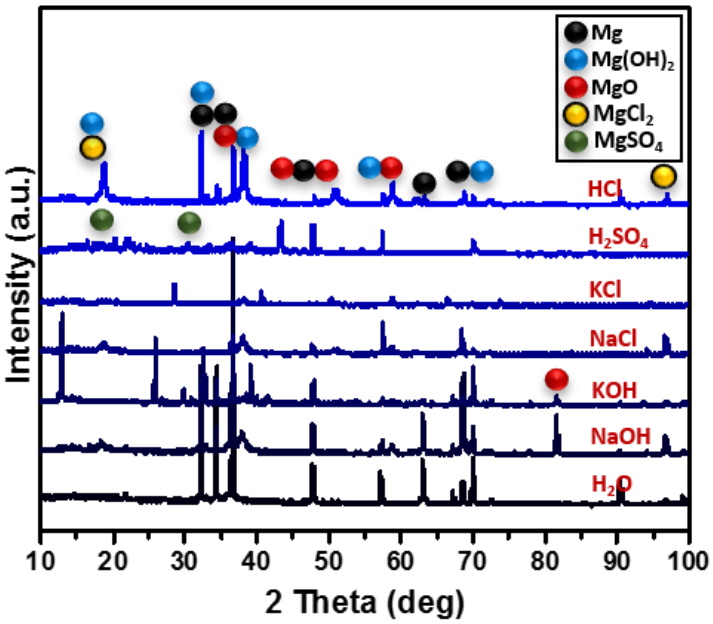

Figure 4.9. XRD spectra of adhering corrosion products/passive films on Mg coupons exposed to different corrodents.

4.2 Investigation of effect of calcination temperature on corrosion resistance of MgO coating

4.2.1 MgO coatings on magnesium alloy: coating formation mechanism and morphology

The dissociation of electrolytic ions (Eq. 1) occurs upon the application of sufficiently high potential using a current source, and this initiates chemical changes around the electrodes. The generated hydroxide ions via water electrolysis (Eq. 2) in turn react with the Mg ions (Mg^{2+}) from dissolved $Mg(NO_3)_2$ to form $Mg(OH)_2$ (s) on the magnesium alloy as cathodic deposits. During the coating calcination process, dehydration of the deposited $Mg(OH)_2$(s) to MgO occurs within the heat charging period (Eq. 3). According to Hashaikeh and Szpunar [18], alternative sources of hydroxide ions could include the simultaneous reduction of oxygen and nitrate. **Figure 4.10** depicts the microstructural morphologies of the as-deposited and calcinated coatings on magnesium alloy; images were recorded without modification of each coating surface.

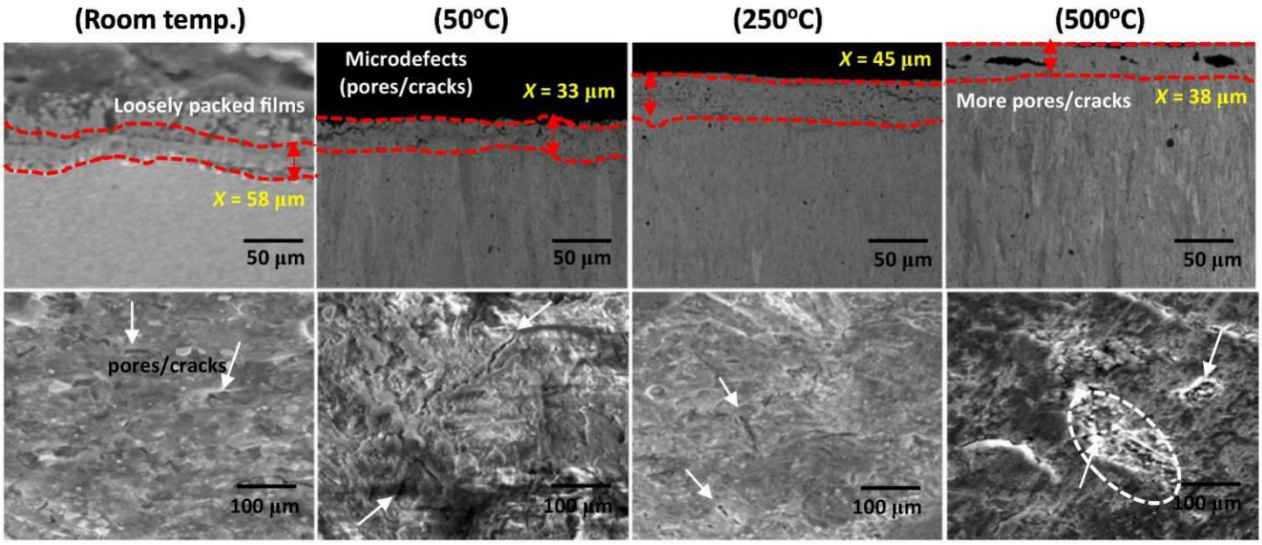

Figure 4.10. The appearance of MgO coatings on magnesium alloy after calcination at different temperatures (First row: cross-sectional SEM morphologies; second row: surface morphology); coating thicknesses (*X*) are also measured in micrometer, µm.

SEM micrographs in the first row depict the cross sections specifically showing inherent pores at interfaces for coatings calcinated at room temperature and at 500°C. These defects are also reflected in the top view SEM images. The multilayered $Mg(OH)_2$ films on the magnesium alloy (calcinated at room temperature) reveal that this coating is relatively incompact with sparse and less crystalline particles. However, the microdefects are gradually removed upon heat treatment (i.e. dehydration of $Mg(OH)_2$) from 50 to 250°C. These calcined coatings are denser and more crystalline compared to the as-coated $Mg(OH)_2$ matrix calcinated at room temperature. Inherent micro pores are again enlarged at 500°C due to possible transformation of stable phases at higher temperature [18,19]. Excessive heat could have deformed the coating microstructure thereby exposing the high diffusion pathways within interphases/solid phases. All coatings are homogenous dark solid deposits, covering the metal surfaces upon drying. Thickness of coating (X) deposits could be controlled by the magnitude of current density [18] as well as the deposition time. In our work , 20 mA/cm^2 and one hour coating deposition time were chosen. Other authors have also reported improved deposit properties at lower low current density and the reduced thicknesses [14,15,18,31]. The calcination process slowly reduces the weight of the coated metal substrate as MgO is formed from $Mg(OH)_2$. Between room temperature and calcination at higher temperatures (50-500°C), values of coating thickness is significantly reduced as the coating microstructures become compact with continuous oxide phases.

$$Mg(NO_3)_{2(aq.)} \rightarrow Mg^{2+}_{(aq.)} + 2NO^{-}_{3(aq.)} \quad (1)$$

$$2H_2O_{(l)} + 2e^{-} \rightarrow H_{2(g)} + 2OH^{-}_{(aq.)} \quad (2)$$

$$Mg(OH)_{2(aq.)} \rightarrow MgO_{(s)} + H_2O_{(l)} \quad (3)$$

4.2.2 Characterization of MgO coatings: XRD and XPS analyses

Figure 4.11a depicts the XRD spectra of coatings calcinated at different temperatures on magnesium alloy. The spectra of these coatings reveal clearly distinct crystallization patterns of the coating particles. For the room-temperature calcined coating, there are few major XRD peaks corresponding to $Mg(OH)_2$ (2θ=18.3 38 and 58°) and Mg (from the base metal) [14,18]. As expected, the calcinated coatings has crystalline structures with MgO on the based metal peaks at specific locations corresponding to 2θ=42.9º (002), 62.6º (220) and 75.0º (200) [14,33]. Other peaks (e.g. peaks of α-Mg) are likely due to the diverse chemical environments within each coating as observed at 2θ values between 31° and 35° and around 70°. In general, these results reveal that crystalline MgO formation was imminent for heat treatment between 50 and 500°C.

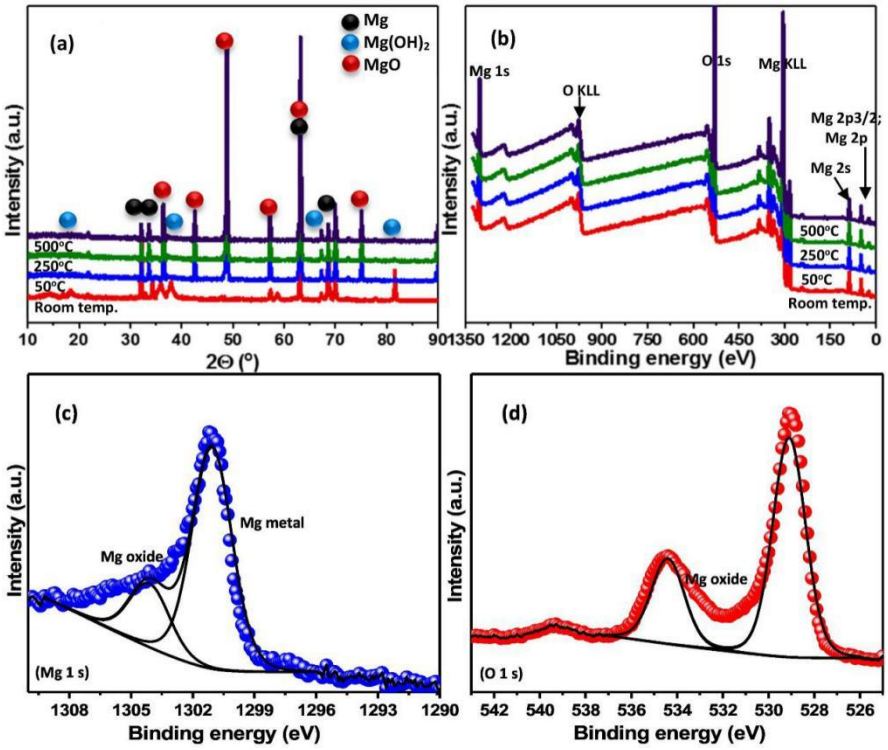

Figure 4.11 XRD (a), XPS wide-scan (b) and XPS high-resolution Mg 1 s (c) and O 1 s (d) spectra of MgO coatings on magnesium alloy substrate calcinated at different temperatures (high-resolution curves were collected for coating calcinated at 250 °C).

The coatings were also investigated using XPS and **Figure 4.11b–d** depicts their wide-scan and high-resolution spectra after applying deconvolution analyses [34]. After analysis more than 90% combined Mg and O was observed to be present within the coatings. Major peaks are displayed on the wide scan spectra. These Mg-O contents relate to deposited coatings on the substrate, with prominent peaks at 1302 eV (Mg 1 s) and 301 eV (Mg KLL) as well as 530 eV (O 1 s) and 980 eV (O KLL), and with no significant binding energy shifts [61]. Their peaks are depicted in **Figure 4.11(c and d)** with the Mg metallic and oxide components both deconvoluted. The peak at 1301.9 eV represents metallic Mg inherent within the based metal while the peak at 1304.8 eV is indicative of the presence of MgO [34]. On the O 1 s spectrum (**Figure 4.11d**), the peak observed at 530.5 eV could be attributed to the formation of Mg-O bonds, and this confirms the presence of the dehydrated product in Eq. 3. The low binding energy peak component at 529 eV may be possibly linked with the O^{2-} ions while the one at the higher energy (534.5 eV) is assigned to loosely bound O atoms on the surface of MgO crystals [64]. The computed values of average Vickers hardness for deposited MgO coatings are presented in **Table 4.2**. The bare metal possessed an average hardness value of 83 HV with increased magnitude obtained for all coated samples. Heat treatment has also show a significant increase of micro hardness due to crystal formation and nucleation. Within this study, the trend in micro hardness is: Room temperature < 50°C < 500°C < 250°C. The highest value of hardness was 359 HV, recorded for MgO coating on Mg substrate calcinated at 250°C and this could be attributed to the formation of stable and dense oxide phases. Lower hardness at 500°C could also be linked with the presence of porous structures within the coating/substrate interface as well as formation of micropores and cracks at higher temperature.

Table 4.2.

Magnitude of Vicker's microhardness for coated Mg samples

Bare Mg	Calcination temperature for coatings			
	Room temperature	50°C	250°C	500°C
83±2 HV	183±9HV	202±3HV	359±4HV	310±3HV

4.2.3 Measuring protective performance of MgO coatings by Tafel polarization

The electrochemical parameters derived from fitting experimental Tafel polarization curves are an effective tool for evaluating the protective performance of coatings. Highly resistive coating systems have lower magnitude of current density. To obtain the relevant parameters (e.g. current density *j*corr) and corrosion potential (*E*corr)), Tafel extrapolation was conducted after identifying the Tafel regions via tangents to the anodic and cathodic curves [65]. In this work, these values are presented in **Table 4.3** for room temperature investigation in 3.5 wt% NaCl corrosive medium. From the polarization curves depicted in **Figure 4.12**, a positive shift in the magnitudes of *E*corr is observed for the coatings as compared to the bare Mg substrate. An approximately 100 mV vs *E*ref shift in *E*corr between the bare and calcinated coatings was recorded while −764.0 mV vs *E*ref was observed for the coating calcinated at room temperature. Since the values of *E*corr for all coatings are positive relative to the bare Mg substrate, it could be concluded that the protective mechanism of MgO coatings against chloride-induced corrosion of Mg substrate was largely an anodic process. These coatings could have acted as a physical barrier against inherent Mg dissolution within the medium. Relative to the bare Mg metal, a steady decrease in the value of

*j*corr was observed in the presence of the coatings after exposure to the corrosive medium for 24 h. The value of *j*corr was reduced for the coatings calcinated between room temperature and 250°C.

Table 4.3.

Electrochemical parameters for MgO coated Mg substrates exposed to 3.5 wt% NaCl corrosive medium following different calcination thermal conditions

Substrates/thermal conditions		Electrochemical impedance spectroscopy						Potentiodynamic polarization technique			
		*R*soln (Ω cm^2)	*R*pore (Ω cm^2)	*Q*c, *Y*o (μF cm^{-2} s$^{-(1-\alpha c)}$)	*R*ct (Ω cm^2)	*Q*dl, *Y*o (μF cm^{-2} s$^{-(1-\alpha c)}$)	$\chi^2 \times 10^{-6}$	*E*corr (mV vs Ref)	*j*corr (μA cm^{-2})	βa (mV/dec)	βc (mV/dec)
Calcinated MgO coatings	500°C	10.2	3161	565.4	239.4	0.47	409.7	-533.0	1.400	505.1	14.1
	250°C	15.6	5037	296.0	330.4	0.14	705.7	-543.0	0.296	393.5	33.8
	50°C	10.3	2387	802.1	193.9	0.97	355.2	-548.0	2.413	59.4	92.3
	Room temp.	14.7	865	2650.7	21.1	13.58	752.8	-764.0	99.20	54.1	171.2
Bare Mg		12.8	-	-	392.5	713.66	478.9	-864.0	298.0	19.9	108.1

χ^2 represents Goodness of Fit; values of α within this work are between ranged between 0.51 and 0.93; the recorded magnitudes of inductive resistance (R_L) and inductance (L) are 152.2 Ω cm^2 and 445.4H.

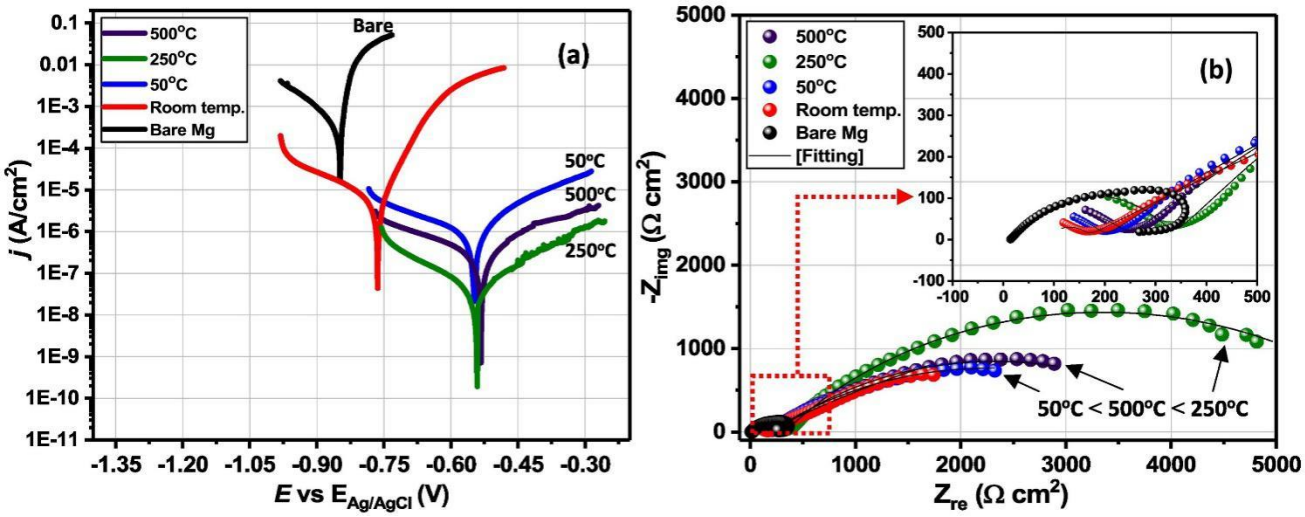

Figure 4.12. Tafel (a) and Nyquist (b) curves for MgO coated Mg substrates calcinated at different temperatures after exposure to 3.5 wt% NaCl corrosive medium at room temperature (the order of enhanced corrosion protection with calcination temperature is: room temperature < 50°C < 500°C < 250°C).

From **Table 4.3**, trend of *j*corr values ranges from 2.413 μA cm^{-2} for coating calcinated at 50°C to 1.400 μA cm^{-2} for the coating calcinated at 500°C while 0.296 μA cm−2 was recorded for coating calcinated at 250°C after immersion in 3.5 wt% NaCl for 24 h. In all, the magnitude of *j*corr for MgO coated Mg substrates is in the order: 250°C < 500°C < 50°C < room temperature. Higher temperature could have initiated phase transformation by deforming the coating microstructure while the internal thermal stress within the coating at 500°C further enlarged inherent MgO coating pores. From these results, increased calcination temperature improved the gross compactness of coating particles hence corrosion resistance. However, at 500°C, recrystallization of the MgO increased coating porosity and more diffusion pathways were created within the interphases of solid coating phases, hence, this reduced barrier performance [19–21]. Chen *et al*. [21] have reported that some calcination conditions are far too extreme for Al-Si composite coatings, depending on the type and distribution of the coating particles. According to

these authors, the Al-Si composite coatings partially (or totally) melt at higher calcination temperatures, from 500°C and after 600°C. In these cases, the calcination process significantly improved corrosion resistance of coatings by enhancing the coating compactness and that limited the permeation rate of corrosive ions and molecules into the specimen [19–21].

4.2.4 Measuring corrosion resistance by impedance spectroscopy

By measuring coating impedance using EIS technique, this method complemented the Tafel technique for characterizing corrosion behaviours of MgO coated Mg substrates in NaCl medium. **Figure 4.12** represents the Nyquist spectra of bare Mg and MgO coated samples calcinated at different temperatures after exposure to 3.5 wt% NaCl solutions for 24 h. Compared with the bare metal, Nyquist curves of the coated Mg substrates are two-time constant semi-circles with high-frequency capacitive loops. The first part of the curve (at higher frequency) depict the polarization resistance of coatings while the second (at lower frequency) is mainly related to charge transfer [23]. Wider impedance capacitive loops denote improved corrosion resistance; and in this work, MgO coating calcinated at 250°C have the highest resistance against corrosion. In addition, appropriate equivalent electric circuit models (**Figure 4.13 a and b**) were used to fit the experimental impedance results presented in the Nyquist curves for coated and bare Mg substrates. This approximation process aids in the adjudication of the corrosion resistance of coatings.

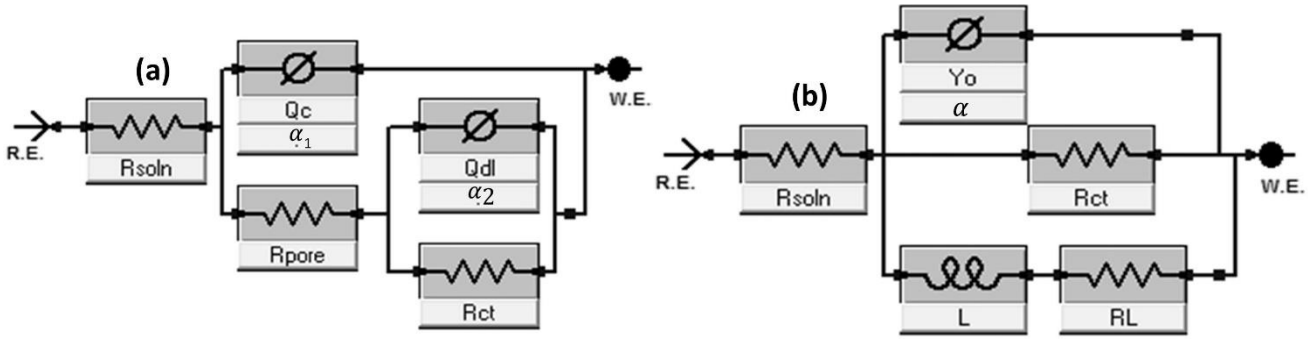

Figure 4.13. Equivalent circuit models used in fitting the experimental impedance for coated (a) and bare (b) Mg substrates. These circuits are made of resistor (solution resistance (*R*soln), pore resistance within coatings (*R*pore), charge transfer resistance (*R*ct) and inductive resistance (*R*L)) and capacitor (coating capacitance (*Q*c) and double layer capacitance (*Q*dl)) components. Constant phase elements (*Q*c and *Q*dl) were introduced to eliminate imperfect capacitive responses from irregular coating surfaces; they also compensate for the deviation from ideal capacitive character.

The ability of the coating to resist the flow of electrolyte currents through pores is depicted as pore resistance (R_{pore}). Decrease in the value of pore resistance marks a coating degradation; the coating calcinated at room temperature has the lowest values of R_{pore} (865Ωcm^2). Values like 2387, 5037 and 3161 in kΩcm^2 were recorded for coatings calcinated at higher temperatures 50°C, 250°C and 500 °C, respectively. With the MgO coatings calcinated at 250°C has the highest R_{pore} values, it could be concluded that this coating has the lowest bulk volume and porosity index, hence it is the highest corrosion resistant [24]. The enhancement of pore resistance due to penetrative chloride pathway is also reflected in the trend of magnitudes of Q_C for every coating. Values of Q_C define the conduction paths for water uptake, ionic migration and salt intrusion within the coatings. Coatings with more compact internal networks absorb fewer corrosive ions and molecules, and in this work, MgO coating had the lowest Q_C value when calcinated at 250°C. The magnitude of Q_C is changing with the calcination temperature of the coating and is the highest at room temperature (2650 nF cm^{-2} s$^{-(1-\alpha c)}$) and then decreases: 50°C (802 nF cm^{-2} s$^{-(1-\alpha c)}$) > 500°C (565 nF cm^{-2} s$^{-(1-\alpha c)}$) > 250°C (296 nF cm^{-2} s$^{-(1-\alpha c)}$). Properly calcinated coatings have compact microstructures,

and this is an important factor for improvement of corrosion resistance. However, at temperatures higher than this temperature, coating phases are transformed, initiating pores within the coatings [19]. For the MgO coating, degradation is observed when a change from amorphous to crystalline structure take place leading to formation of grain boundaries (that act as diffusion paths for corrosive ions) [20,21,25–27]. At the coating/metal interface, *R*ct.*Q*dl describes the beginning of coating disbanding at lower frequencies. The order of reducing magnitude of *R*ct with the calcination temperature of coating is room temperature ($21\Omega cm^2$) < 50°C ($193\Omega cm^2$) < 500°C ($239\Omega cm^2$) < 250°C ($330\Omega cm^2$). At this juncture, 250°C is revealed as the optimum calcination temperature for highly protective MgO coatings on Mg substrate and this is also reflected in the values of *Q*dl. This quantity (*Q*dl) increases with the calcination temperature of coating: room temperature (13 $\mu F\ cm^{-2}\ s^{-(1-\alpha c)}$) > 50°C (0.97 $\mu F\ cm^{-2}\ s^{-(1-\alpha c)}$) > 500°C (0.47 $\mu F\ cm^{-2}\ s^{-(1-\alpha c)}$) > 250°C (0.14 $\mu F\ cm^{-2}\ s^{-(1-\alpha c)}$). The trend of the impedance data shows that the presence of these oxide coatings protects Mg substrate [24]. The Bode modulus and phase angle curves of all MgO coated Mg substrates as well as bare metal are presented in **Figure C1**. A comparison of the process conditions and protective performance of MgO coatings within this study and the results reported for some metallic substrates in the literature are presented in **Table 4.4**.

Table 4.4.

Comparison of the process conditions and protective performance of MgO coatings within this study and those reported for some metallic substrates in literature

Coating/ substrate type	Coating technique/ method	Calcination temperature	Comparative corrosion protective performances	Conditions for improved coating performance	[Ref.]
MgO coating/ magnesium alloy	Cathodic electrodeposition in $Mg(NO_3)_2$ and heat treatment	Different Calcination temperatures; between room temperature and 500°C	j_{corr} values of MgO coating (at 250°C calcination temperature) lowers more	Excess dehydration led to compact internal microstructures and continuous oxide coating layers.	*This study

			than 300 times compared with the bare magnesium alloy. Coating (or pore) resistance is 5037 Ωcm^2 at this temperature in 3.5 wt% NaCl	Enhanced protective performance was observed only at the optimum calcination temperature (250°C).	
MgO coating/ magnesium alloy	Anodization in KOH solution	MgO conversion from $Mg(OH)_2$ at 450°C	Compared with the bare alloy, the j_{corr} values of calcinated MgO coatings formed in 6 and 10 M KOH, lowered more than 10 to 100 times, respectively	The rate of nucleation and growth of coatings was enhanced in 10 M KOH; coatings possessed improved barrier performance at this concentration.	[14]
$Mg(OH)_2$/MgO coating/ Mg alloy	Alternative current impedimetric method in KOH solution	No heating	Mg dissolution was controlled by charge transfer process at the active region while $Mg(OH)_2$ deposition dominated the passive region of the impedance spectrum	Mg was directly oxidized to MgO as a secondary oxidation process controlled by charge transfer and diffusion of water	[15]
MgO coating/ Ni superalloy	Cathodic electrodeposition in $Mg(NO_3)_2$ and heat treatment	Coated specimens were fired at (700-1100°C) in air	Designed for high temperature oxidation resistance applications; corrosion tests not investigated	Coating deposition decreased with time and as temperature increases; optimum calcination temperature was 200°C.	[18]
MgO coating/ magnesium alloy	Anodic electrodeposition in KOH solution and heat	Annealing treatment at 450°C in air	j_{corr} lowers more than 100 times compared with	MgO coatings were produced by	[28]

	treatment		the bare magnesium alloy	anodic electrodeposition in 10 M KOH alkaline solution at constant potential of 1 V for 2 h, and calcinated at 450°C for 6 h in air.	

*The present study uses two complementary methods (Electrochemical impedance spectroscopic and potentiodynamic polarization techniques) for corrosion testing.

4.2.5 Correlating thermal calcination mechanism and corrosion resistance of coatings

Less protective MgO coatings subsequently fail due to percolation of fluids, and enhanced corrosion resistance was observed at the optimum calcination temperature judging from the electrochemical results after chloride treatment. In this work, inter-diffusion between the coating substrate and interfaces led to disbonding of oxide layers formed during dehydration as presented in the calcination mechanism at different thermal conditions in **Figure 4.14**. The internal tensile stress was produced in the process of electrodeposition because the hydrogen produced during the whole deposition process was occluded in the deposits. The calcination process initiated the formation of compact internal microstructures with continuous oxide layers due to dehydration-assisted internal tensile stress release at 250°C [19–21].

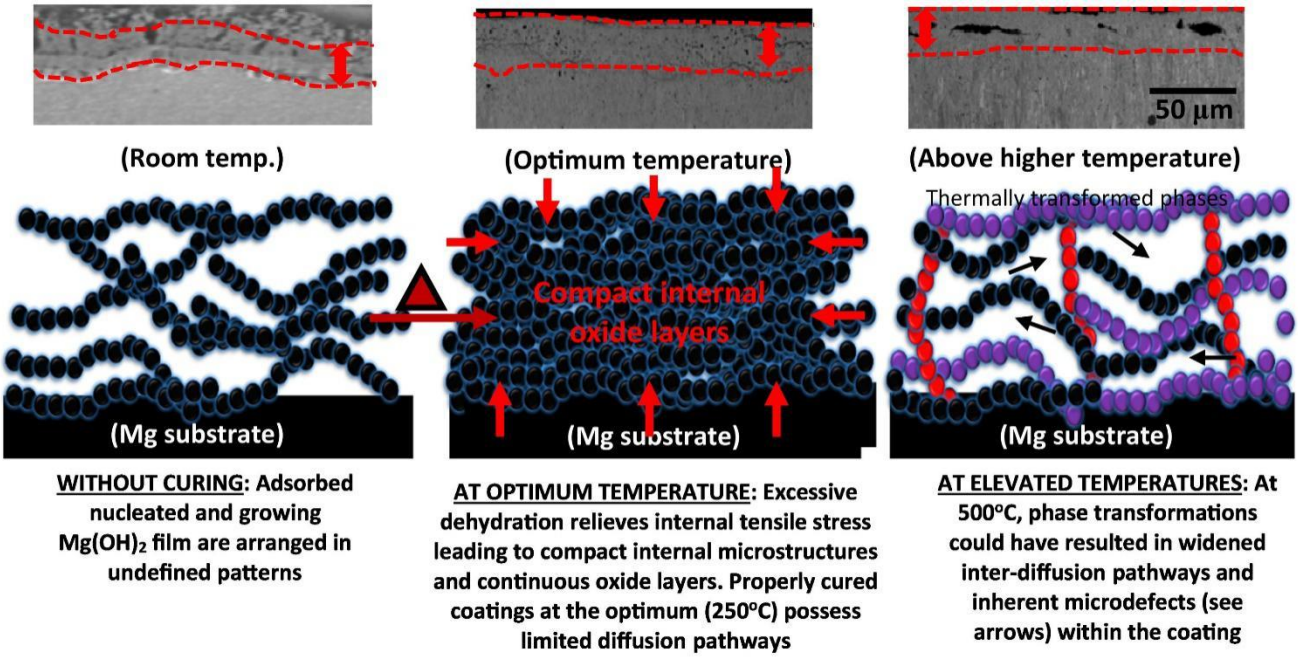

Figure 4.14. Proposed calcination mechanism for MgO coatings on magnesium alloy substrate at different thermal conditions.

The presence of stable passive and crystalline oxide layers inhibit fluid uptake towards the metal surface as well as the formation of more cathodic Mg sites by blocking diffusion pathways. At elevated temperatures (e.g. 500°C in this work), the distortion of their internal multilayered microstructures led to phase transformations as well as the enhancement of inherent conducting pathways. The microcracks (and other defects; e.g. micropores) observed on **Figure 4.10** for MgO coating calcinated at 500°C is a clear evidence of the consequence of overheating [19–22]. In all, the corrosion resistance of these MgO coating is significantly influenced by the thermal calcination mechanism.

4.3 Proposing corrosion mechanism

It should be noted that on Mg and its alloys, there is always a spontaneously/naturally formed surface film mainly consisting of MgO and $Mg(OH)_2$ [43]. The corrosion products formed on the surface are based on following reactions [2]:

$$Mg \rightarrow Mg^{2+} + 2e^- \quad (1)$$

$$2H_2O + 2e^- \rightarrow H_2 + 2OH^- \quad (2)$$

$$Mg^{2+} + 2OH^- \rightarrow Mg(OH)_2 \quad (3)$$

$$Mg(OH)_2 + Cl^- \rightarrow MgCl_2 + 2OH^- \quad (4)$$

Based on the reaction (1) (anodic reaction) and (2) (cathodic reaction), Mg transforms to stable Mg^{2+} ion and then the cathodic reaction occurs which produces the hydroxide ion. Magnesium hydroxide are formed as the Mg^{2+} ion reacts with hydroxide ion. As the formed $Mg(OH)_2$ acts as a protection film, the degradation rate of Mg sample declines and corrosion products precipitate on its surface. In addition, the corrosion products which contain $Mg(OH)_2$ also fill the corrosion pits and therefore result in further reduction of the corrosion rate. According to reaction (4), later chloride ion reacts with $Mg(OH)_2$ protection film on the surface and produces $MgCl_2$ which has higher solubility than that of $Mg(OH)_2$. Because of the chloride ion reaction, the dissolution rate and formation rate of the $Mg(OH)_2$ protection film are different. As a result, it could be concluded that chloride ion decreases the corrosion resistance of magnesium alloy.

Corrosion of the substrate can easily occur in the film-free areas. When a specimen is immersed in a corrosive solution, the solution including aggressive ions (e.g. Cl^- cations) will get into through-pores and eventually reach the substrate/ coating interface, where the solution will be in contact with the bare substrate surface in the film-free areas. After the concentration of Cl^- increases above a critical threshold (supposed to be much lower than 5 wt%), the substrate Mg is rapidly dissolved into the pore solution in the through-pores from the film-free areas of the substrate, which will make the pore solution saturated with $Mg(OH)_2$. Hence, the substrate magnesium alloy surface is actually exposed to a $Mg(OH)_2$ saturated NaCl solution in the coating through-pores.

Based on the above corrosion process description, the corrosion of an anodized magnesium alloy can be schematically illustrated in **Figure 4.15**. The naturally/spontaneously formed porous surface film is a discontinuous layer, and the film-free areas can be treated as kinds of film pores like those in anodized coatings.

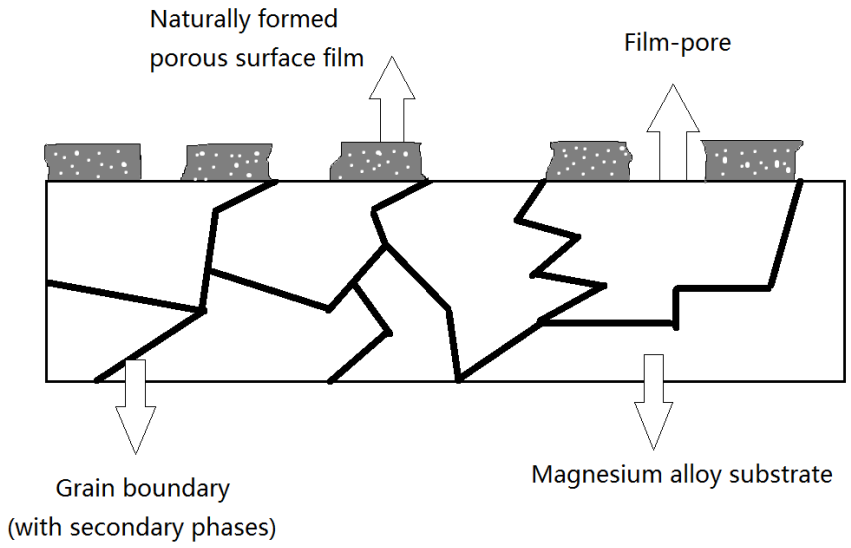

Figure 4.15. The proposed corrosion mechanism for magnesium alloy

CHAPTER FIVE

SUMMARY, CONCLUSIONS AND RECOMMENDATIONS

5.1 Summary

The degradation behaviour of ZX10 magnesium alloy in 1 M corrosive media and the protective performance of MgO coatings electrodeposited on ZX10 magnesium alloy followed by subsequent calcination at defined temperature range were investigated. First, the magnesium alloy samples were immersed in seven different solutions at room temperature for several days. Then the corrosion behaviour of magnesium alloy is investigated using SEM, EBSD, XRD spectra and electrochemical analysis. Magnesium alloy degradation has revealed varying rates of corrosion and passivation within a range of pH of corrosion media. The chemistry and diffraction phases of adhering corrosion products as well as their surface morphologies have also been identified. The corrosion products are mainly $Mg(OH)_2$ and MgO. In the second part, the MgO coatings electrodeposited on magnesium alloy were calcinated at defined temperature range in order to investigate their different corrosion resistance. During the calcination process, excess dehydration leads to compact internal microstructures and continuous coating layers. Properly cured coatings at the optimum temperature (250°C) have limited diffusion pathways against corrosive ions and molecules; this has been elaborately studied for changes in electrochemical parameters with calcination temperature. At elevated temperatures (around 500°C), phase transformations resulted in widened inter-diffusion pathways and inherent microdefects within coatings. The defects (e.g. microcracks and micropores) observed for MgO coatings calcinated at 500°C are a clear evidence of the consequence of over-calcination. A modelled calcination mechanism, as it relates to

corrosion resistance at low and high thermal conditions for MgO coatings, has been proposed from exhaustive experimental evidence.

5.2 Conclusions

The following were the conclusions drawn from this project:

1. ZX10 magnesium alloy degradation has revealed varying rates of corrosion and passivation within a range of pH of corrosion media.
2. The corrosion behaviour of magnesium alloy is investigated; increasing Mg corrosion rate follows this trend: acid> salt > alkali (Mg corrodes more in the acidic media).
3. Localized corrosion behaviour has been observed by SEM while the electrochemical impedance spectroscopy and potentiodynamic polarization techniques reveals increased anodic polarization and charge transfer.
4. The chemistry and the phase compositions of adhering corrosion products as well as their surface morphologies have been identified. The corrosion products are mainly $Mg(OH)_2$ and MgO.
5. Mg must have corroded uniformly within each corrodent over extended duration; however, the early stages of magnesium alloy corrosion reveal localized passivation at the grain boundaries.
6. The protective MgO coatings were successfully applied on surface of ZX10 magnesium alloys by cathodic electrodeposition and subsequent calcination.
7. Calcination temperature influences mechanical properties and corrosion resistance of MgO coatings as the calcination relieves internal stress leading to compact microstructures and continuous oxide layers.

8. MgO coatings calcinated at 250°C largely increased the corrosion resistance of Mg alloy and this could be confirmed by the reduction of current density (from 298 $\mu A/cm^2$ for bare Mg to 0.296 $\mu A/cm^2$).
9. MgO are over-calcinated at 500°C and microdefects and internal diffusion pathways are enlarged.

5.3 Recommendations for future work

1. In order to investigate the interaction of the cracks formed after corrosion with grain boundaries, high resolution TEM should be used.

2. As temperature is an important factor in the corrosion studies, in addition to room temperature, different corrosion temperature, including 0°C, 10°C, 30°C and 40°C should be chosen to investigate the effect of corrosion temperature on degradation process of magnesium alloy.

3. In addition to the hardness, other mechanical properties of the ZX10 magnesium alloy without coating, such as strength, ductility and toughness are also influenced by heat treatment. Therefore, the effect on these properties should be investigated by conducting tests like tensile test.

4. Calcination time also influences the corrosion resistance of MgO coating and the effect of time should be studied by choosing different heating duration, such as sixty minutes,two hours and three hours at the same temperature.

REFERENCES

[1] Alvarez-Lopez, M., Pereda, M. D., Del Valle, J. A., Fernandez-Lorenzo, M., Garcia-Alonso, M. C., Ruano, O. A., & Escudero, M. L. "Corrosion behaviour of AZ31 magnesium alloy with different grain sizes in simulated biological fluids." *Acta biomaterialia* 6.5 (2010): 1763-1771.

[2] Bakhsheshi-Rad, H. R., Hamzah, E., Medraj, M., Idris, M. H., Lotfabadi, A. F., Daroonparvar, M., & Yajid, M. A. M. "Effect of heat treatment on the microstructure and corrosion behaviour of Mg–Zn alloys." *Materials and Corrosion* 65.10 (2014): 999-1006.

[3] Han, L., Li, X., Bai, J., Xue, F., Zheng, Y., & Chu, C. "Effects of flow velocity and different corrosion media on the in vitro bio-corrosion behaviours of AZ31 magnesium alloy." *Materials Chemistry and Physics* 217 (2018): 300-307.

[4] Ma, C., Peng, G., Nie, L., Liu, H., & Guan, Y. "Laser surface modification of Mg-Gd-Ca alloy for corrosion resistance and biocompatibility enhancement." *Applied Surface Science* 445 (2018): 211-216.

[5] Ghanbari, A., Khiabani, A. B., Zamanian, A., Yarmand, B., & Mozafari, M. "The competitive mechanism of plasma electrolyte oxidation for the formation of magnesium oxide bioceramic coatings." *Mater. Today Proc.* 5 (2018): 15677-15685.

[6] Zheng, Y. F., Gu, X. N., & Witte, F. "Biodegradable metals." *Materials Science and Engineering: R: Reports* 77 (2014): 1-34.

[7] Salahinejad, E., Hadianfard, M. J., Macdonald, D. D., Mozafari, M., Walker, K. J., Rad, A. T.,& Tayebi, L. "Surface modification of stainless steel orthopedic implants by sol–gel ZrTiO4 and ZrTiO4–PMMA coatings." *Journal of biomedical nanotechnology* 9.8 (2013): 1327-1335.

[8] Sepahvandi, A., Moztarzadeh, F., Mozafari, M., Ghaffari, M., & Raee, N. "Photoluminescence in the characterization and early detection of biomimetic bone-like apatite formation on the surface of alkaline-treated titanium implant: State of the art." *Colloids and Surfaces B: Biointerfaces* 86.2 (2011): 390-396.

[9] Mina, A., Caicedo, J., Aperador, W., Mozafari, M., & Caicedo, H. "Evaluation of Mechanical and Tribological Properties of Coatings for Stainless Steel." *Applied Nanoindentation in Advanced Materials* 1 (2017): 269-286.

[10] Pawar, S., Slater, T. J. A., Burnett, T. L., Zhou, X., Scamans, G. M., Fan, Z., G.E Thompson., & Withers, P. J. "Crystallographic effects on the corrosion of twin roll cast AZ31 Mg alloy sheet." *Acta Materialia* 133 (2017): 90-99.

[11] Hussein, R., Northwood, D., & Nie, X. "The effect of processing parameters and substrate composition on the corrosion resistance of plasma electrolytic oxidation (PEO) coated magnesium alloys." *Surface and Coatings Technology*237 (2013): 357-368.

[12] Gao, J. H., Guan, S. K., Ren, Z. W., Sun, Y. F., Zhu, S. J., & Wang, B. "Homogeneous corrosion of high pressure torsion treated Mg–Zn–Ca alloy in simulated body fluid." *Materials Letters* 65.4 (2011): 691-693.

[13] Narayanan, T. S., Park, I. S., & Lee, M. H. "Strategies to improve the corrosion resistance of microarc oxidation (MAO) coated magnesium alloys for degradable implants: Prospects and challenges." *Progress in Materials Science* 60 (2014): 1-71.

[14] Lei, T., Ouyang, C., Tang, W., Li, L. F., & Zhou, L. S. "Preparation of MgO coatings on magnesium alloys for corrosion protection." *Surface and Coatings Technology* 204.23 (2010): 3798-3803.

[15] Cai, Z., Lu, D., Li, W., Liang, Y., & Zhou, H. "Study on anodic oxidation of magnesium in 6 M KOH solution by alternative current impedance." *international journal of hydrogen energy* 34.1 (2009): 467-472.

[16] Durdu, S., & Usta, M. "Characterization and mechanical properties of coatings on magnesium by micro arc oxidation." *Applied Surface Science* 261 (2012): 774-782.

[17] Tang, H., & Gao, Y.. "Preparation and characterization of hydroxyapatite containing coating on AZ31 magnesium alloy by micro-arc oxidation." *Journal of Alloys and Compounds* 688 (2016): 699-708.

[18] Hashaikeh, R., & Szpunar, J. A. "Electrolytic processing of MgO coatings." *Journal of Physics: Conference Series*. Vol. 165. No. 1. IOP Publishing, 2009.

[19] Yildiz, R. A., Göksenli, A., Yüksel, B. H., Muhaffel, F., & Aydeniz, A. "Effect of annealing temperature on the corrosion resistance of electroless produced Ni-BW coatings." *Advanced Materials Research*. Vol. 651. Trans Tech Publications, 2013.

[20] Jin, Y., Fan, J., Mou, K., Wang, X., Ding, Q., Li, Y., & Liu, C. "Effect of heat treatment on the structure and properties of electrolessly deposited Ni-W-Cr-P alloy coatings on aluminum alloy." *KOVOVE MATERIALY-METALLIC MATERIALS* 49.4 (2011): 279-285.

[21] Chen, C., Lu, C., Feng, X., & Shen, Y. "Effects of annealing on Al–Si coating synthesised by mechanical alloying." *Surface Engineering*33.7 (2017): 548-558.

[22] Serin, I. G., Göksenli, A., Yüksel, B., & Yildiz, R. A. "Effect of annealing temperature on the corrosion resistance of electroless Ni-B-Mo coatings." *Journal of Materials Engineering and Performance* 24.8 (2015): 3032-3037.

[23] Cui, M., Xu, C., Shen, Y., Tian, H., Feng, H., & Li, J. "Electrospinning superhydrophobic nanofibrous poly (vinylidene fluoride)/stearic acid coatings with excellent corrosion resistance." *Thin Solid Films* 657 (2018): 88-94.

[24] Ammar, S., Ramesh, K., Ma, I. A. W., Farah, Z., Vengadaesvaran, B., Ramesh, S., & Arof, A. K. "Studies on SiO2-hybrid polymeric nanocomposite coatings with superior corrosion protection and hydrophobicity." *Surface and Coatings Technology* 324 (2017): 536-545.

[25] Gao, Y. E., Zhao, L., Yao, X., Hang, R., Zhang, X., & Tang, B. "Corrosion behaviour of porous ZrO2 ceramic coating on AZ31B magnesium alloy." *Surface and Coatings Technology* 349 (2018): 434-441.

[26] Yuan, J., Yuan, R., Wang, J., Li, Q., Xing, X., Liu, X., & Hu, W. "Fabrication and corrosion resistance of phosphate/ZnO multilayer protective coating on magnesium alloy." *Surface and Coatings Technology* 352 (2018): 74-83.

[27] Shahri, Z., Allahkaram, S. R., Soltani, R., & Jafari, H. "Study on corrosion behaviour of nano-structured coatings developed on biodegradable as cast Mg–Zn–Ca alloy by plasma electrolyte oxidation." *Surface and Coatings Technology* 347 (2018): 225-234.

[28] Lei, T., Ouyang, C., Tang, W., Li, L. F., & Zhou, L. S. "Enhanced corrosion protection of MgO coatings on magnesium alloy deposited by an anodic electrodeposition process." *Corrosion science* 52.10 (2010): 3504-3508.

[29] Kartsonakis, I. A., Balaskas, A. C., Koumoulos, E. P., Charitidis, C. A., & Kordas, G. C. "Incorporation of ceramic nanocontainers into epoxy coatings for the corrosion protection of hot dip galvanized steel." *Corrosion science* 57 (2012): 30-41.

[30] Song, G. "Recent progress in corrosion and protection of magnesium alloys." *Advanced engineering materials* 7.7 (2005): 563-586.

[31] Liu, Y., Hang, R., Zhao, Y., Bai, L., Sun, Y., Yao, X., ... & Hang, R. "The effects of annealing temperature on corrosion behaviour, Ni2+ release, cytocompatibility, and antibacterial ability of Ni-Ti-O nanopores on NiTi alloy." *Surface and Coatings Technology* 352 (2018): 175-181.

[32] Zhang, D. Q., Gao, L. X., & Zhou, G. D. "Synergistic effect of 2-mercapto benzimidazole and KI on copper corrosion inhibition in aerated sulfuric acid solution." *Journal of Applied Electrochemistry* 33.5 (2003): 361-366.

[33] Li, J., Hu, W., Hao, L., Gao, B., Wu, S., Zhang, J., ... & Fan, H. "Electron-induced secondary electron emission of Zn-doped MgO/Au composite film." *Materials Letters* 229 (2018): 360-363.

[34] Aksoy, S., Caglar, Y., Ilican, S., & Caglar, M. "Sol–gel derived Li–Mg co-doped ZnO films: Preparation and characterization via XRD, XPS, FESEM." *Journal of Alloys and Compounds* 512.1 (2012): 171-178.

[35] Rabizadeh, T., & Asl, S. K. "Casein as a natural protein to inhibit the corrosion of mild steel in HCl solution." *Journal of Molecular Liquids* 276 (2019): 694-704.

[36] Jiang, L., Xu, F., Xu, Z., Chen, Y., Zhou, X., Wei, G., & Ge, H. "Biodegradation of AZ31 and WE43 magnesium alloys in simulated body fluid." *Int. J. Electrochem. Sci* 10 (2015): 10422-10432.

[37] Xu, Z., Eduok, U., & Szpunar, J. "Effect of annealing temperature on the corrosion resistance of MgO coatings on Mg alloy." *Surface and Coatings Technology* 357 (2019): 691-697.

[38] Hsu, C. S., Nazari, M. H., Li, Q., & Shi, X. "Enhancing degradation and corrosion resistance of AZ31 magnesium alloy through hydrophobic coating." *Materials Chemistry and Physics* 225 (2019): 426-432.

[39] Znamenskii, M. S. "Metallic osteosynthesis by means of an apparatus made of resorbing metal." *Khirurgiia* 12.2 (1945): 60-63.

[40] Singh, I.B., Singh, M, & Das, S. "A comparative corrosion behaviour of Mg, AZ31 and AZ91 alloys in 3.5% NaCl solution." *Journal of Magnesium and Alloys* 3.2 (2015): 142-148.

[41] Miao, H., Huang, H., Shi, Y., Zhang, H., Pei, J., & Yuan, G. "Effects of solution treatment before extrusion on the microstructure, mechanical properties and corrosion of Mg-Zn-Gd alloy in vitro." *Corrosion Science* 122 (2017): 90-99.

[42] Huang, L., Wang, K., Wang, W., Yuan, J., Qiao, K., Yang, T., & Li, T. "Effects of grain size and texture on stress corrosion cracking of friction stir processed AZ80 magnesium alloy." *Engineering Failure Analysis* 92 (2018): 392-404.

[43] Song, G. L., & Shi, Z. "Corrosion mechanism and evaluation of anodized magnesium alloys." *Corrosion Science* 85 (2014): 126-140.

[44] Bakhsheshi-Rad, H. R., Hamzah, E., Ismail, A. F., Aziz, M., Daroonparvar, M., Saebnoori, E., & Chami, A. "In vitro degradation behaviour, antibacterial activity and cytotoxicity of TiO2-MAO/ZnHA composite coating on Mg alloy for orthopedic implants." *Surface and Coatings Technology* 334 (2018): 450-460.

[45] Liu, Y., Curioni, M., & Liu, Z. "Correlation between electrochemical impedance measurements and corrosion rates of Mg-1Ca alloy in simulated body fluid." *Electrochimica Acta* 264 (2018): 101-108.

[46] Selvam, M., Saminathan, K., Siva, P., Saha, P., & Rajendran, V. "Corrosion behaviour of Mg/graphene composite in aqueous electrolyte." *Materials chemistry and physics* 172 (2016): 129-136.

[47] Witte, F., Hort, N., Vogt, C., Cohen, S., Kainer, K. U., Willumeit, R., & Feyerabend, F. "Degradable biomaterials based on magnesium corrosion." *Current opinion in solid state and materials science* 12.5-6 (2008): 63-72.

[48] Kim, B. H., Ha, S. H., Yoon, Y. O., Lim, H. K., Kim, S. K., & Kim, D. H. "Effect of Ca addition on selective oxidation of Al3Mg2 phase in Al-5 mass% Mg alloy." *Materials Letters* 228 (2018): 108-111.

[49] Ghali, E. "Activity and passivity of magnesium (Mg) and its alloys." *Corrosion of Magnesium Alloys*. Woodhead Publishing, 2011. 66-114.

[50] Pan, P., Chen, H., Liang, Z., & Zhao, Q. "Deposition and corrosion characteristics of liquid-solid droplets on tubular corrosion probes in desulfurized flue gas." *Engineering Failure Analysis* 90 (2018): 129-140.

[51] Alves, H., Koster, U., Aghion, E., & Eliezer, D. "Environmental behaviour of Magnesium and Magnesium Alloys." *Materials Technology* 16.2 (2001): 110-126.

[52] Chen, J., Wang, J., Han, E., Dong, J., & Ke, W. "States and transport of hydrogen in the corrosion process of an AZ91 magnesium alloy in aqueous solution." *Corrosion Science* 50.5 (2008): 1292-1305.

[53] Nordlien, J. H., Ono, S., Masuko, N., & Nis, K. "Morphology and structure of oxide films formed on magnesium by exposure to air and water." *Journal of the Electrochemical Society* 142.10 (1995): 3320-3322.

[54] Xia, S. J., Birss, V. I., Rateick Jr, R. G., & Bend, I. N. "Anodic Oxide Film Formation at Magnesium Alloy WE43." *Surface Oxide Films: Proceedings of the International Symposium*. Vol. 2003. The Electrochemical Society, 2004.

[55] Song, G. L., & Atrens, A. "Corrosion mechanisms of magnesium alloys." *Advanced engineering materials* 1.1 (1999): 11-33.

[56] Luan, B. L., Yang, D., Liu, X. Y., & Song, G. L. "Corrosion protection of magnesium (Mg) alloys using conversion and electrophoretic coatings." *Corrosion of Magnesium Alloys*. Woodhead Publishing, 2011. 541-564.

[57] Reddy, C. M., Gaston, R. S., Weikart, C. M., & Yasuda, H. K. "Influence of surface pretreatment and electrocoating parameters on the adhesion of cathodic electrocoat to the Al alloy surfaces." *Progress in organic coatings* 33.3-4 (1998): 225-231.

[58] Palsson, N. S., Bunchoo, N., Wongpisan, W., & Chanthapan, S. "Effect of liquid magnesium on high temperature failure of heat resistant alloy." *Engineering Failure Analysis* 79 (2017): 296-312.

[59] Subramanian, C. "Localized pitting corrosion of API 5L grade A pipe used in industrial fire water piping applications." *Engineering Failure Analysis* 92 (2018): 405-417.

[60] Li, C. F., Wang, M. J., Ho, W. H., Li, H. N., & Yen, S. K. "Effects of electrolytic MgO coating parameters on corrosion resistance of AZ91D magnesium alloy." *Journal of The Electrochemical Society* 158.2 (2011): C11-C16.

[61] Yin, D., Niu, X., Zhang, K., Wang, J., & Cui, Y. "Preparation of MgO doped colloidal SiO2 abrasive and their chemical mechanical polishing performance on c-, r-and a-plane sapphire substrate." *Ceramics International* 44.12 (2018): 14631-14637.

[62] Song, G-L. "Corrosion electrochemistry of magnesium (Mg) and its alloys." *Corrosion of Magnesium alloys*. Woodhead Publishing, 2011. 3-65.

[63] Asgari, H., Szpunar, J. A., Odeshi, A. G., Zeng, L. J., & Olsson, E. "Effect of grain size on high strain rate deformation of rolled Mg–4Y–3RE alloy in compression." *Materials Science and Engineering: A* 633 (2015): 92-102.

[64] Das, P. S., Bakuli, S., Biswas, I., Mallik, A. K., Dey, A., Mukherjee, S., ... & Mukhopadhyay, A. K. "RGO/MgO hybrid nanocomposites with high specific capacitance." *Ceramics International* 44.1 (2018): 424-432.

[65] Ding, J. H., Zhao, H. R., Zheng, Y., Zhao, X., & Yu, H. B. "A long-term anticorrsive coating through graphene passivation." *Carbon* 138 (2018): 197-206.

[66] Hartman, M., Trnka, O., & Veselý, V. (1994). Thermal dehydration of magnesium hydroxide and sintering of nascent magnesium oxide. *AIChE journal*, *40*(3), 536-542.

[67] Hourani, M., & Wedian, F. (2000). The effect of adatoms on the corrosion rate of copper. *Corrosion science*, *42*(12), 2131-2144.

APPENDIX A

Standard Operating Procedure for LaboPol-20 manual polishing machine located in room 2C26, Engineering Building, University of Saskatchewan, Canada.

1. Introduction

The LaboPol-20 manual polishing machine is used to grind and polish metallic samples for metallographic etching or use as a substrate in thin film deposition. This equipment was designed and constructed by Struers Company. This procedure details the Standard Operating Procedure which I developed for safe operation of the equipment as part of my M.Sc. work.

2. Safety

1) **Physical Hazard**

• No sample under 5mm thick can be held by hand, thin specimens must be mounted onto a holder either by the procedure described in Mat0004 for heat activated glue, or by water proof double sided adhesive (tape).

• The polishing wheels rotate at a high speed and represent a potential entanglement hazard.

• The Si-C discs and diamond abrasives are an abrasion hazard; care should be taken to avoid scraping your skin.

• Liquid on a rotating disc could potentially splash into your eye; therefore safety glasses are required for this procedure

2) **Chemical and Toxicological Hazards**

• The diamond slurries and lubricants are skin, eye and lung irritants and their MSDS's or PDS's should be consulted prior to polishing.

• The water based Diamond suspensions can be disposed of in a general sink and their waste does not need to be collected as hazardous waste.

• For alcohol based diamond suspensions (used with water sensitive materials such as magnesium) Mat0025 must be followed with respect to waste collection and safety protocol, SOP Mat0025 takes precedence with respect to any contradiction between this SOP and Mat0025.

3. LaboPol-20 manual polishing machine

Figure A.1 LaboPol-20 manual polishing machine

4. Procedure

4.1 Stage 1: Setting up

1. Depending on the starting roughness of the specimen, some pre-grinding on the belt grinder in the heat treatment lab may be required. If so, follow the procedure outlined in the belt grinder SOP.
2. Depending on the size of the specimen (thickness in particular) it may be required to be cold mounted or “temporarily stub mounted” (Mounting Metallographic Samples SOP, Mat0004)

4.2 Stage 2: Procedure

1. See the accompanying tables for a general guide on the abrasives and discs/cloths to be used, these depend on the type of specimen being prepared.
2. Coarse Grinding:

   a. Belt grinder – Not recommended

      i. Pull out some new Si-C paper and turn on the water to the belt grinder.

      ii. Slowly push and pull the specimen across the wetted Si-C paper in a back and forth motion, do not apply a lot of force or you will round the specimen.

      iii. Repeat until you can see linear grooves of all the same size in the same direction that you are grinding.

      iv. If a second grit of SiC paper is required rotate the specimen 90° and repeat the above steps i->iii, rinsing with running water between grits.

b. Rotational polishing wheel – SiC paper

i. Using either:

1. a PSA backed Si-C paper applied directly to a brass polishing platen, or to a MD-Rondo disk (blue) for use on a magnetic platen. NEVER apply a PSA backed paper or cloth to a MD-Gekko disk (red).

2. or a non-PSA backed Si-C foil on a MDGekko (red disk). Turn on the polishing wheel to low speed, then to HIGH speed (if higher speed is required).

ii. Turn on the flowing water and wet the entire abrasive paper.

iii. Rotate the specimen in the same direction as the wheel rotates until the surface finish is entirely the grit being used.

c. Rotational polishing wheel – MD Piano

i. Place the appropriate Disc onto a magnetic backed platen and insert the platen onto the polishing head, and turn to LOW speed, then High speed if required.

ii. Turn on the flowing water and wet the entire abrasive paper.

iii. Rotate the specimen in the same direction as the wheel rotates until the surface finish is entirely the grit being used.

3. Rinse the specimen in running water.

a. NOTE: with alcohol or oil based suspensions the water must be collected as hazardous waste so a water squirt bottle should be used over a funnel draining into a waste disposal container. Close the sample chamber

4. Rinse the specimen with alcohol and blow dry.

5. Fine Grinding: MD-System.

    a. Place the appropriate Disc onto a magnetic backed platen and insert the platen onto the polishing head, and turn to LOW speed.

    b. Pour some abrasive onto the Disc (do not overuse the abrasive as it is very expensive).

    c. Rotate the specimen in the same direction as wheel rotation, indicated by >> in the tables.

6. Rinse the specimen in running water.

    a. NOTE: with alcohol or oil based suspensions the water must be collected as hazardous waste so a water squirt bottle should be used over a funnel draining into a waste disposal container.

7. Rinse the specimen with alcohol and blow dry.

8. Coarse Polishing: MD-System.

    a. Place the appropriate Disc onto a magnetic backed platen and insert the platen onto the polishing head, and turn to LOW speed.

    b. Pour some abrasive onto the Disc (do not overuse the abrasive as it is very expensive).

    c. Rotate the specimen in the same direction as wheel rotation, indicated by >> in the tables

9. Rinse the specimen in running water

a. NOTE: with alcohol or oil based suspensions the water must be collected as hazardous waste so a water squirt bottle should be used over a funnel draining into a waste disposal container.

10. Rinse the specimen with alcohol and blow dry.

11. Final Polish: MD-System.

a. Place the appropriate Disc onto a magnetic backed platen and insert the platen onto the polishing head, and turn to LOW speed.

b. Pour some abrasive onto the Disc (do not overuse the abrasive as it is very expensive).

c. Rotate the specimen in the same direction as wheel rotation, indicated by >> in the tables.

12. Rinse the specimen in running water.

a. NOTE: with alcohol or oil based suspensions the water must be collected as hazardous waste so a water squirt bottle should be used over a funnel draining into a waste disposal container.

13. Rinse the specimen with alcohol and blow dry.

4.2 Stage 3: Clean up

1. The MD-Largo, MD Allegro and MD-Piano discs must be fully rinsed with running water prior to being returned to the storage container; in addition the back side should be dried with paper towel. These discs can be cleaned under running water with the nylon brushes provided and labeled for use on Ferrous or Non-Ferrous discs only.

a. NOTE: with alcohol or oil based suspensions the water must be collected as hazardous waste so a water squirt bottle should be used over a funnel draining into a waste disposal container.

2. The MD-Dac , MD-Mol, MD-Dur, MD-Chem and MD-Nap discs can be returned immediately after use, simply wipe the metal side dry if it is wet and return to the storage container in the appropriate labeled shelf.

3. Ensure that all abrasive containers are closed tightly and returned to the appropriate shelf or drawer.

5. **Highlights**

When polishing magnesium alloy samples which are water sensitive specimens, always using alcohol based diamond suspensions and pure ethyl alcohol. Alcohol based suspensions must be treated as hazardous waste, and must not be allowed to drain into a sink or floor drain.

APPENDIX B

Other experiment devices used in present study

1 Buehler ABRASIMET 2 abrasive cutter

Figure B.1 Buehler ABRASIMET 2 abrasive cutter

2 Hitachi SU6600 SEM and EBSD/EDS

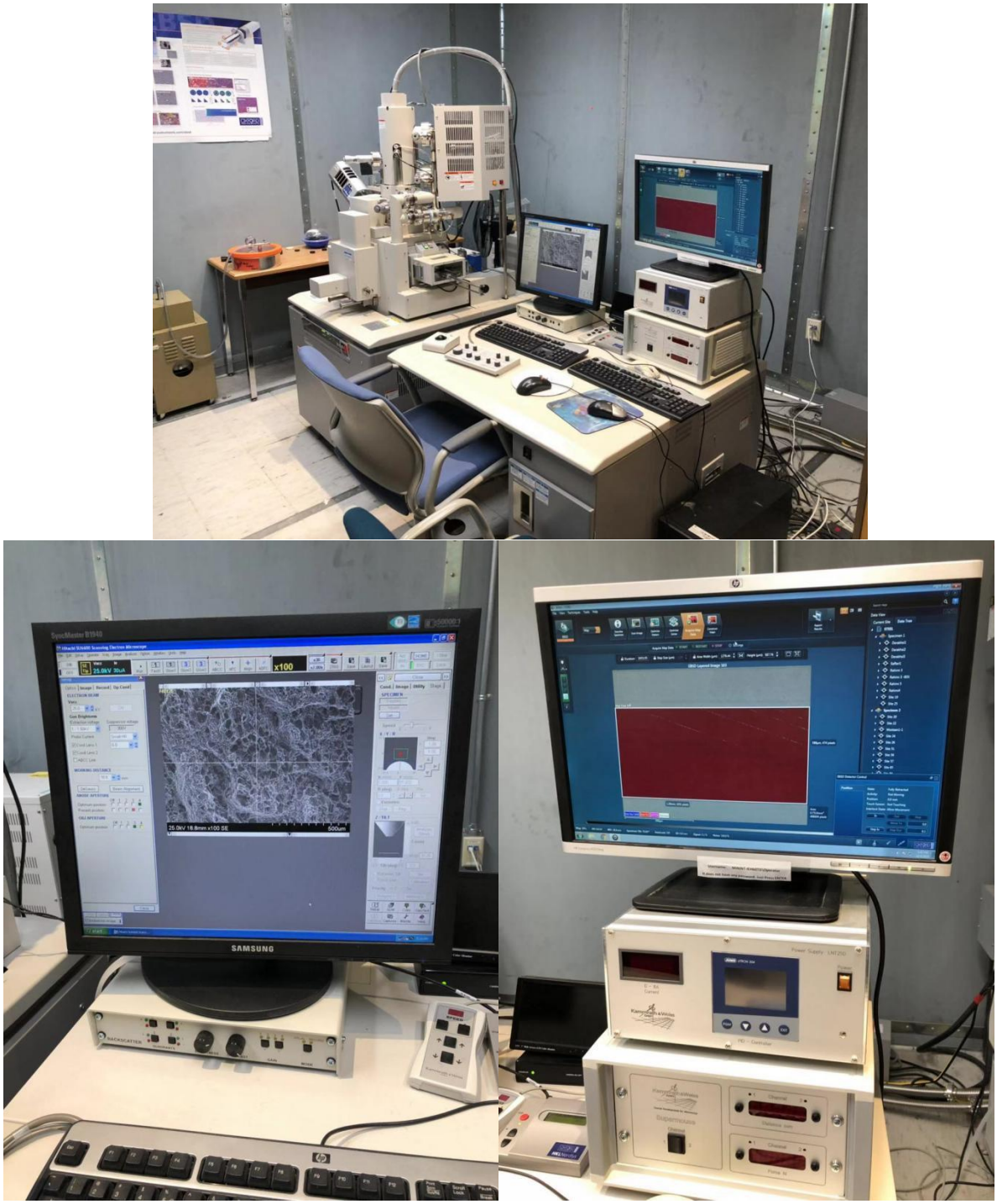

Figure B.2 Hitachi SU6600 SEM and EBSD/EDS

APPENDIX C

Supplementary information

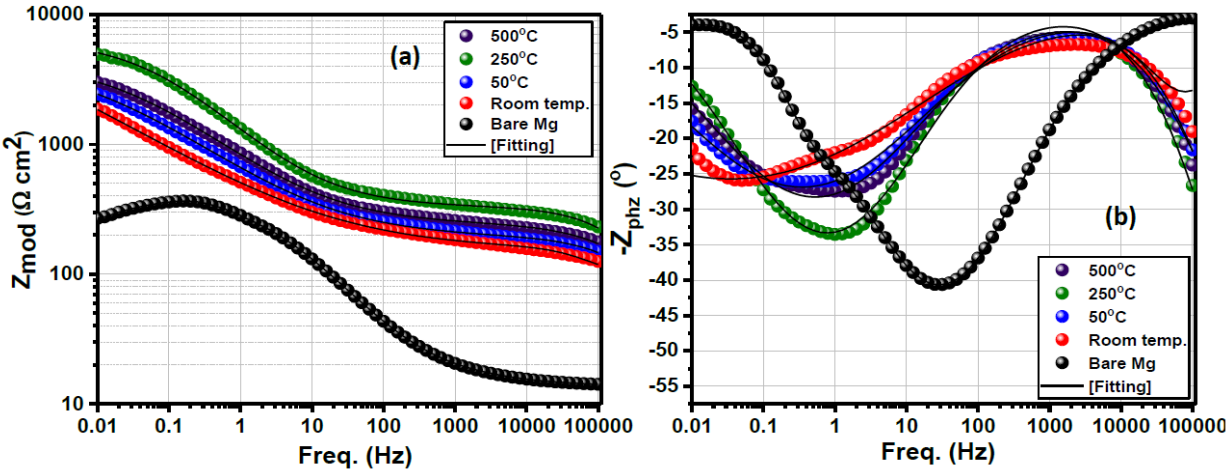

Figure C.1. Bode modulus and phase angle curves of bare Mg and MgO coated Mg substrates calcinated at different temperatures exposed to 3.5 wt% NaCl corrosive medium at room temperature